



# Prospects and challenges of mini-LED, OLED, and micro-LED displays

En-Lin Hsiang, SID Student Member<sup>1</sup> | Zhiyong Yang, SID Student Member<sup>1</sup>  | Qian Yang, SID Student Member<sup>1</sup> | Yi-Fen Lan<sup>2</sup> | Shin-Tson Wu, SID Fellow<sup>1</sup> 

<sup>1</sup>College of Optics and Photonics, University of Central Florida, Orlando, Florida, USA

<sup>2</sup>AU Optronics Corp., Hsinchu, Taiwan

## Correspondence

Shin-Tson Wu, College of Optics and Photonics, University of Central Florida, Orlando, FL 32816, USA.  
Email: swu@creol.ucf.edu

## Funding information

a.u.Vista, Inc., Grant/Award Number: 65018A64

## Abstract

Recently, “liquid crystal display (LCD), organic light-emitting diode (OLED), or micro-light-emitting diode (LED): who wins?” is a heated debatable question. In this review article, we provide a comprehensive overview of these three promising display technologies through nine display performance indicators, including ambient contrast ratio, motion picture response time, viewing angle and angular color shift, color gamut, resolution density, power consumption, cost, lifetime, and thin profile and panel flexibility. The advantages and disadvantages of each technology are analyzed, and their future perspectives are discussed.

## KEYWORDS

high-dynamic range, micro-LED, mini-LED backlit LCD, OLED

## 1 | INTRODUCTION

Display is an important human-machine interface. Its widespread applications range from smart watches, smartphones, pads, computers, TVs, to vehicles, just to name a few. Recently, the competition between liquid crystal displays (LCDs)<sup>1</sup> and organic light-emitting diode (OLED)<sup>2</sup> displays has become increasingly fierce. Being an emissive display, the red, green, and blue (RGB) OLED panel exhibits a perfect dark state, vivid colors, and thin and flexible profile. Its applications have gradually migrated from smartphones to tablets and laptops. In parallel, white OLED displays with color filters have also grasped an important market share in large-screen TVs. To keep up the competition and maintain the dominating market in terms of shipment volume, two-dimensional (2D) local dimming mini-light-emitting diode (LED) backlight units are used in LCDs to improve their contrast ratio, peak brightness, bit depth, and power consumption. This way, mini-LED backlit LCD (mLCD)

can meet the high-dynamic-range (HDR) requirements. According to Dolby Research standard, an HDR display should exhibit a peak brightness > 4000 nits, dark state < 0.005 nit, and at least 10 bits of gray levels. In the meantime, micro-LED ( $\mu$ LED) display<sup>3,4</sup> with high peak brightness, true black state, and long lifetime is emerging as a potentially disruptive technology. A fair comparison between these three display technologies would inspire each camp to strengthen its own advantages and improve its shortcomings.

Liquid crystal (LC) is a nonemissive display, which means a backlight unit is required. After over five decades of extensive materials research, device innovations, and heavy investment in advanced manufacturing technologies, thin-film transistor (TFT) LCDs have reached mature stage in all aspects. Some key challenges, such as the viewing angle, response time, and color gamut, have been overcome. Since 2000s, TFT LCDs have gradually displaced the bulky cathode ray tubes (CRTs) as a dominant flat panel display technology.<sup>5-7</sup>

As an emissive display, OLED offers several unique advantages, such as ultrathin profile, unprecedented

En-Lin Hsiang and Zhiyong Yang contributed equally to this work.

contrast ratio (CR), fast material response time, and vivid colors.<sup>8,9</sup> After more than three decades of continuous development in new materials, emission mechanisms, device structures, and manufacturing technologies, OLED's performance has also reached a mature stage and has become a strong contender to LCDs. Moreover, its ultrathin profile enables bendable, rollable, and foldable OLED displays.

Besides all the above-mentioned advantages of OLED displays,  $\mu$ LED displays exhibit another big advantage, which is high brightness with an ultrasmall chip. As a result, the aperture ratio can be as small as 1%, which means 99% of the pixel area can be covered by either black matrix (for sunlight readable displays) or by transparent material (for transparent displays). Currently, commercialization of  $\mu$ LED displays still faces several challenges, such as (1) high cost due to complicated manufacturing process, including mass transfer and pixel repair; (2) wavelength shift and external quantum efficiency (EQE) variation under different driving currents, which increases the difficulty of addressing  $\mu$ LED displays with a precise brightness control and color uniformity; and (3) reduced efficiency as the chip size decreases, which compromises the power consumption.<sup>10–13</sup>

In this review paper, we briefly describe the device configurations and operation principles of these three technologies. Next, we use following nine metrics to fairly compare their performances: (1) high ambient CR (ACR); (2) fast motion picture response time (MPRT) to suppress motion image blur; (3) wide viewing angle with negligible angular color shift; (4) wide color gamut; (5) low power consumption, which is particularly important for battery-powered mobile displays; (6) high-resolution density, especially for augmented reality (AR) and virtual reality (VR) applications; (7) low cost; (8) long lifetime; and (9) thin profile, freeform, and flexibility.

## 2 | DEVICE STRUCTURES

### 2.1 | Liquid crystal displays

Two types of backlight units, edge lit and direct lit, have been widely used in TFT LCDs. The former offers a thin profile, which is particularly attractive for portable displays such as smartphones and notebook computers. However, in this configuration, the image quality improvement by adapting 2D local dimming technology is limited due to inadequate zone number and blurred zone boundary.<sup>14,15</sup> Recently, with the rapid development of mini-LED technology, direct-lit backlights with local dimming functions can also be made quite thin.<sup>16–18</sup> As a result, both HDR and thin profile can be achieved simultaneously.

In addition to mini-LED, which usually has thousands of local dimming zones, dual-cell LCDs composed of two LCD panels (subcell and main cell)<sup>19,20</sup> have also been proposed and commercialized to achieve 2D local dimming. The subcell can be a low-resolution (e.g.,  $1920 \times 1080$ ) black-and-white LCD panel, whereas the main cell is a high-resolution (e.g.,  $3840 \times 2160$ ) full-color LCD panel. Because of double modulation layers, such a dual-cell LCD is equivalent to a mLED with about two million local dimming zones. As a result, high CR ( $>1,000,000:1$ ) and high bit depth ( $>14$  bits) can be achieved by a low driving voltage (5 V).<sup>20</sup> Compared with mLCD, although dual cell offers about  $1000\times$  more dimming zone number, some issues such as thicker profile, reduced optical efficiency, image splitting,<sup>21</sup> and moiré effect<sup>22</sup> remain to be tackled.

In an LCD, each pixel works as a light shutter to control the transmittance of the backlight. Four popular LC operation modes, depending on the molecular alignments and electrode configurations, have been developed: (1) twisted nematic (TN) mode,<sup>23</sup> (2) vertical alignment (VA) mode,<sup>24</sup> (3) in-plane switching (IPS) mode,<sup>25</sup> and (4) fringe-field switching (FFS) mode.<sup>26</sup> Multidomain VA (MVA) mode has been widely used in large TVs due to its high on-axis CR (CR  $> 5000:1$ ) and fast response time<sup>27,28</sup>; FFS mode has been widely adopted in mobile applications due to its high transmittance, robustness to touch pressure, wide viewing angle, and weak color shift.<sup>29,30</sup> Therefore, MVA and FFS modes are selected here as two examples to illustrate the basic operation principles of LCDs.

Figure 1A depicts the FFS device structure. In an FFS cell, the LC directors are initially homogeneously aligned between two substrates. The top substrate has LC alignment layer but no ITO electrode. In the bottom substrate, pixel electrodes are formed above the common electrode. The cell is sandwiched between two crossed linear polarizers, and the transmission axis of the bottom polarizer is parallel to the rubbing direction of the LC director. Thus, without any voltage ( $V = 0$ ), the incident light after passing through the bottom polarizer maintains the same linear polarization when traversing the LC layer and is absorbed by the crossed analyzer. In this way, a decent dark state can be obtained. When the applied voltage exceeds a threshold ( $V_{th}$ ), because the lateral field is non-uniform in both horizontal and vertical directions, the LC directors are reoriented into two serial TN cells with a reversed twist.<sup>31</sup> Thus, the incident light experiences some phase retardation and transmits through the crossed polarizers. It should be noted that the transmittance of the FFS cell is position dependent due to non-uniform horizontal fields. The strongest horizontal field occurs at the pixel electrode edges, making the LC directors twist more and thus leading to a higher transmittance.<sup>32</sup> At the centers of electrodes and gap, the

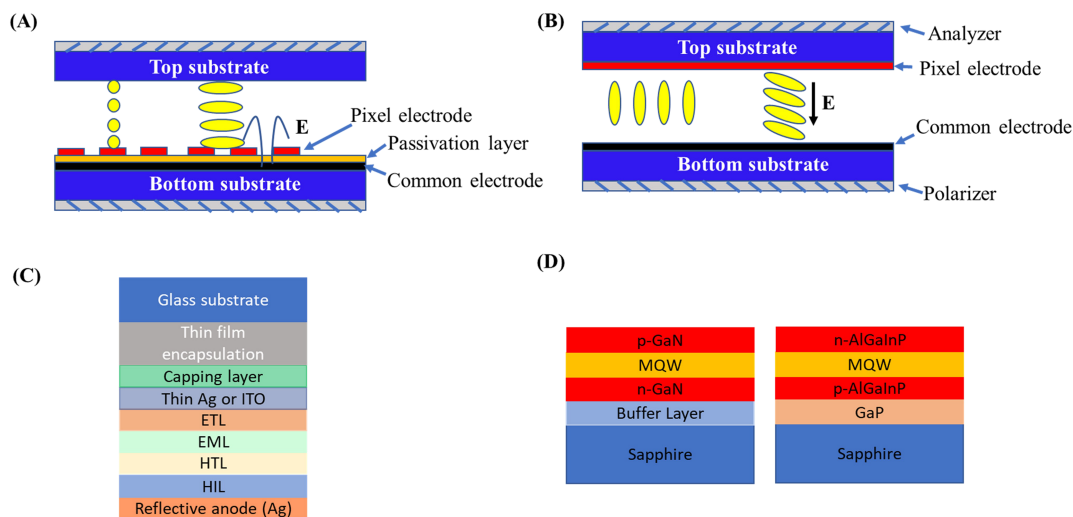


**FIGURE 1** Schematic diagram of (A) fringe-field switching (FFS) liquid crystal display (LCD), (B) vertical alignment (VA) LCD, (C) organic light-emitting diode (OLED) display, and (D) micro-light-emitting diode ( $\mu$ LED) display. The liquid crystal (LC) director orientations are shown in the voltage-off (left) and voltage-on (right) states. ETL, electron transport layer; HTL, hole transport layer; MQW, multiple quantum well

horizontal fields are the weakest, and the vertical fields dominate, making the LC directors twist less and thus leading to a lower transmittance. In an FFS LCD, both positive and negative dielectric anisotropy ( $\Delta\epsilon$ ) LC materials can be used.<sup>33</sup> The negative  $\Delta\epsilon$  LC gives a higher transmittance and weaker flickering<sup>34</sup> but slower response time because of its higher viscosity than the positive counterpart. For MVA, Figure 1B shows that the LC with a negative  $\Delta\epsilon$  is aligned along the vertical direction when  $V = 0$ , giving rise to an excellent dark state. With  $V > V_{th}$ , the LC directors are gradually reoriented by the longitudinal field so that the incident light can transmit through the crossed analyzer.

## 2.2 | Organic light-emitting diodes

For an emissive display, no external light source is required; thus, the device structure is simple. In an OLED display,<sup>35,36</sup> the emission layer is contained in an optical cavity as shown in Figure 1C. The multilayer OLED device consists of (1) a reflective anode (Ag), (2) hole injection layer, (3) hole transport layer (HTL), (4) emission layer, (5) electron transport layer (ETL), (6) semitransparent cathode (Mg:Ag), and (7) an organic capping layer. The microcavity is formed by the semitransparent top electrode and the reflective bottom electrode.<sup>37,38</sup> In an RGB OLED, HTL and ETL have different thicknesses to achieve different cavity resonance wavelengths, thereby improving color purity, whereas the thin organic capping layer above the semitransparent cathode helps to enhance the optical efficiency.<sup>39–41</sup> In addition,

the alternating stacks thin-film encapsulation<sup>42</sup> is used to prevent the moisture and oxygen from deteriorating the organic material. Based on the emission mechanisms, three major types of OLED devices have been demonstrated: (1) fluorescent OLED, (2) phosphorescent OLED, and (3) thermally activated delayed fluorescent OLED (TADF-OLED).<sup>2,43–46</sup> Each device has its own advantages and disadvantages. In terms of emission efficiency, the internal quantum efficiency (IQE) of fluorescent OLED is initially limited to 25% and is further increased to 62.5% through triplet-triplet annihilation (TTF-OLED). For a phosphorescent OLED, its IQE can reach 100%; however, a heavy metal is required to incorporate with organic emitter, resulting in an increased cost. For TADF-OLED, after removing the heavy metal atoms, its IQE can still maintain 100%. Thus, the molecular design has greater flexibility. In addition to efficiency, lifetime is another key factor for OLED devices. The multiquasiparticle interaction caused by the long exciton lifetime in TADF-OLED and phosphorescent OLED decreases their operation time, especially for blue OLEDs.<sup>47,48</sup> Therefore, for active-matrix OLED (AMOLED) applications, red and green phosphorescent emitters are the main choices because of their high IQE and long lifetime, whereas TTF-OLED is mostly used for blue emitters due to its longer lifetime than the blue phosphorescent OLED.<sup>49</sup>

## 2.3 | Micro-LEDs

In  $\mu$ LED displays, red LEDs are usually produced by growing AlGaInP epitaxial layers on a GaAs substrate, whereas

green and blue LEDs are fabricated from the GaN-based multiple quantum well (MQW) LED structure grown on a sapphire substrate. The device structure of conventional flip-chip  $\mu$ LED chip is shown in Figure 1D. For a display panel size  $> 2$  in., the  $\mu$ LED are divided into millions of individual chips. After that, the “pick and place” process through elastomer stamping, electrostatic/electromagnetic transfer, laser assisted transfer, or fluid self-assembly is implemented to transfer individual  $\mu$ LED chip to the display substrate.<sup>50–54</sup> However, until now, the transfer yield and defect management are still challenging.

For small-size ( $< 2$  in.) display applications, two methods have been proposed to assemble the backplane driver circuitry and LED array: flip-chip bonding and wafer bonding.<sup>55–58</sup> For flip-chip bonding, the  $\mu$ LED is fabricated on the LED substrate, and the metal bonding ball is prepared on the complementary metal-oxide-semiconductor (CMOS) substrate. After that, two wafers are aligned and bonded by thermal-compression method. However, the pixel size is limited to around  $10 \mu\text{m}$  in this method. For wafer-bonding style, the LED epi is firstly bonded to the silicon driver. Then, the  $\mu$ LED is directly fabricated on the CMOS wafer. Therefore, the alignment is not required during the bonding process. The pixel size can be reduced to less than  $5 \mu\text{m}$ .

### 3 | PERFORMANCE METRICS

In the following sections, we discuss the above-mentioned nine performance metrics for LCD, mLCD, OLED, and  $\mu$ LED displays.

#### 3.1 | Ambient contrast ratio

HDR usually refers to a display with peak brightness  $> 1000$  nits, black state  $< 0.005$  nits, and over 10-bit gray levels.<sup>59</sup> However, a display is rarely used at completely dark ambient, so here, we focus on a more realistic ACR. The CR of an emissive display such as OLED and  $\mu$ LED can exceed  $10^6:1$  in a dark room, but in practical applications, the effective CR is substantially affected by the ambient light and surface reflectivity of the display panel. The ACR is defined as<sup>60,61</sup>

$$\text{ACR} = \frac{L_{\text{on}} + L_{\text{am}} \times R_L}{L_{\text{off}} + L_{\text{am}} \times R_L}, \quad (1)$$

where  $L_{\text{on}}$  ( $L_{\text{off}} \approx 0$ ) represents the on (off)-state luminance of the display,  $L_{\text{am}}$  is the ambient luminance, and  $R_L$  is the luminous ambient reflectance of the display panel.

To determine the ACR of a display, the brightness and ambient reflectance of the display panel is measured and simulated. As the ambient light impinges on the display panel, there will be some reflection from the front surface ( $R_1$ ). The transmitted light may further be reflected by the components in the display panel ( $R_2$ ). For LCDs, the ambient light is mainly reflected by the front glass or protective layer, whereas the transmitted light is mostly absorbed by the crossed polarizers. Thus, we can neglect  $R_2$  in our analysis. For OLED displays, the front surface reflection  $R_1$  still exists. In addition, the metal electrodes in the OLED devices cause a strong reflection ( $R_2$ ). As a result, a broadband circular polarizer composed of a linear polarizer and a half-wave plate and a quarter-wave plate is commonly used to minimize the ambient reflection.<sup>62</sup> Such a broadband circular polarizer works well at normal direction. As the viewing angle increases, light leakage gradually increases, leading to a degraded CR. The influence of light leakage from circular polarizer on ACR has been analyzed previously.<sup>63</sup> Although the circular polarizer can significantly suppress the ambient reflection from metal electrodes, it not only absorbs nearly 50% of the emitted light but also limits the flexibility of the OLED panel. Several approaches have been proposed to reduce the ambient reflection of OLED panels, such as black cathodes, destructive interference microcavity, and well-designed black matrix.<sup>64–68</sup> However, the trade-off between high optical efficiency and low ambient reflectance remains.

For  $\mu$ LED displays, the bottom metal electrodes also have a high reflectance. In addition, in comparison with GaN-based green and blue LEDs, the AlGaInP-based red LEDs have a stronger absorption in the green and blue spectral regions, which results in a lower ambient reflectance. The simulated reflection spectrum from RGB LED chips illuminated by D-65 white light source is plotted in Figure 2. It is noteworthy that the relatively low reflectance of GaN-based LED in the blue spectral range is mainly due to the absorption from Au-based electrode. The average luminous ambient reflectance of GaN-based LED and AlGaInP-based red LED is about 67% and 30%, respectively.

However, the aperture ratio of a  $\mu$ LED display is usually small. Thus, only a fraction of the ambient light will be reflected by the LED, and the rest is absorbed by the area covered with black matrix. From Equation 1, a display with high peak brightness and low ambient reflectance would exhibit a high ACR. Here, we take some large-size TVs as examples. It is worth noting that a large-size  $\mu$ LED TV is usually tiled by several small-size  $\mu$ LED modules. Under a typical 50% average picture level (APL), the peak brightness of Vizio 65-in. LCD TV (P-Series Quantum X, 2020) is 991 nits, LG 65-in. OLED TV is



302 nits (CX, 2020), and  $\mu$ LED display is 2333 nits.<sup>69,70</sup> Here, the APL represents the percentage of the display that is lit up compared with a full white display. The peak brightness of the display depends on the APL of the displayed image. For example, when APL = 10%, the peak brightness of the LG OLED display, Vizio LCD, and  $\mu$ LED display increases to 813, 2043, and 2777 nits, respectively.

Under a checker-board pattern, the LCD's CR is 5,078:1, and when the local dimming function is enabled (200 local dimming zones in the 65-in. TV), the CR increases to 14,345:1. If the number of local dimming zone increases, such an mLCD's CR can also be improved dramatically (e.g.,  $10^6$ :1). The CR of the OLED and  $\mu$ LED displays we studied here is set at  $10^6$ :1. The calculated ACR at normal viewing angle as a function of different ambient lighting conditions for three display technologies is illustrated in Figure 3. For a fair comparison, the same antireflection coating ( $R_1 = 1.5\%$ ) is applied to all the display panels. In addition, as mentioned above, the  $R_2$  of the LCD is negligible. For OLED displays, the light

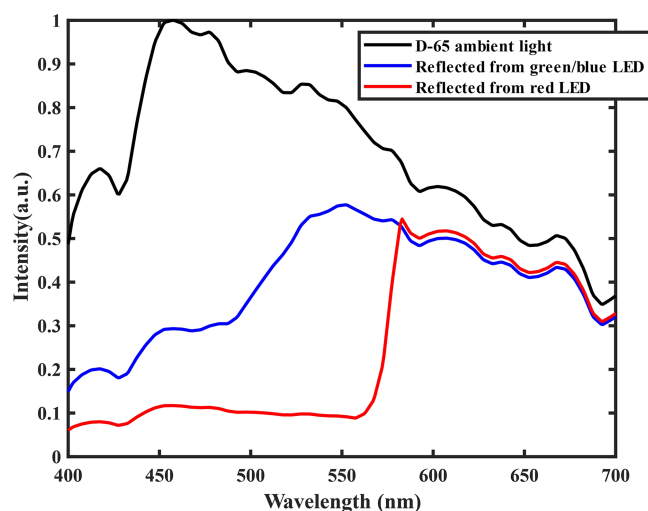


**FIGURE 2** The intensity spectra of D-65 ambient light and the reflected ambient light spectra by AlGaInP-based light-emitting diode (LED) and InGaN-based LED

leakage from the circular polarizer (CP) increases as the viewing angle increases,<sup>63</sup> but at normal viewing angle, it is also negligible. Regarding to  $\mu$ LED displays, the ambient reflection also consists of two parts:  $R_1$  and  $R_2$ . Here,  $R_2$  is mainly from the ambient light passing through the aperture, which in turn is reflected by the  $\mu$ LED chips. The ambient reflection of the RGB  $\mu$ LED chips are shown in Figure 2. In Figure 3, the aperture ratio of the  $\mu$ LED display is assumed to be 1%.

As Figure 3 depicts, ACR decreases sharply and then gradually saturates as the ambient light brightness increases. Under all ambient lighting conditions, the  $\mu$ LED display with a high peak brightness and high intrinsic CR keeps the highest ACR. Unlike  $\mu$ LED display, the ACR of OLED decreases dramatically as the ambient light increases mainly due to its limited peak brightness. From Figure 3A, the crossover point for OLED and LCD occurs at around 20 lux. Below 20 lux, OLED shows a much higher ACR than LCD, but the situation is reversed as the ambient illuminance exceeds 20 lux. This is because the dark level (signal) of the display panel is washed out by the surface reflection (noise) of the ambient light. The ACR comparison between displays under APL = 10% is also plotted in Figure 3B. If we consider a 10% APL, then the crossover point increases to 60 lux. A typical family room lighting is about 100 lux, and an office lighting is about 300–500 lux.

### 3.2 | Motion picture response time

Even the response time of an LCD (ms) is much slower than that of OLED ( $\mu$ s) and LED displays (ns), we should not conclude that LCD will suffer more severe motion blurs than the other two emissive displays. This is because, unlike impulse-type CRT displays, in a hold-type display (active-matrix LCD, OLED, and  $\mu$ LED), the visual perception of a moving object depends not only on the pixel response time but also on the TFT frame rate ( $f$ ) and duty ratio. Thus, MPRT is a more representative way

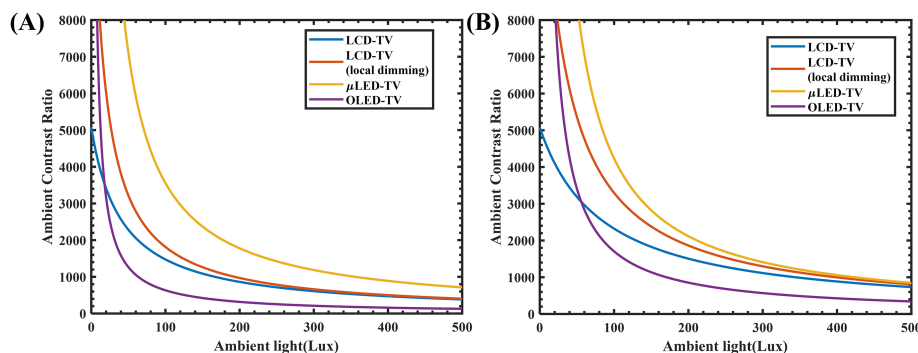


**FIGURE 3** Calculated normal angle ambient contrast ratio (ACR) as a function of different ambient light conditions for liquid crystal display (LCD) (Vizio), mini-light-emitting diode (LED) backlit LCD (mLCD) (Vizio with 200 dimming zones), micro-LED ( $\mu$ LED) (1% aperture ratio), and organic light-emitting diode (OLED) (LG CX) TVs at (A) average picture level (APL) = 50% and (B) APL = 10%. Panel surface reflection ( $R_1$ ) is 1.5%

to describe the image blurs. The widely accepted MPRT is jointly determined by the pixel response time ( $\tau$ ) and frame time ( $T_f = 1/f$ ) as<sup>71–75</sup>

$$MPRT = \sqrt{\tau^2 + (0.8T_f)^2}. \quad (2)$$

A high frame rate helps reduce the MPRT of a display panel, thereby suppressing motion blurs. However, a high frame rate decreases the pixel addressing time and increases the burden on the driving circuit design, especially for high-resolution displays, and the benefit of increasing frame rate gradually saturates. On the other hand, at a specific frame rate, say 120 Hz, reducing the pixel response time will cause the MPRT to first decrease linearly and then gradually saturate onto  $0.8 \times T_f$ . For OLED and  $\mu$ LED displays, their intrinsic fast response time (approximately a few microseconds for OLED and nanoseconds for LED) helps to achieve  $MPRT \approx 0.8 \times T_f$ . However, for an LCD, to make its MPRT in the saturation region, the LC response time should be less than 2 ms. Such a fast response time can be achieved by using a thin cell gap, low viscosity LC material, or the overdrive method.<sup>76–78</sup>

Here, we take a display with 120-Hz frame rate as an example to compare the MPRT of the three display technologies. If the LC response time is faster than 2 ms, the MPRT of the TFT LCD is almost the same as that of OLED and  $\mu$ LED displays. Chen et al.<sup>75</sup> also verified that the MPRT of a VA LC cell with an average gray-to-gray response time of 1.29 ms is 6.88 ms, which is comparable with the MPRT of OLED displays (6.66 ms). Even if we increase the frame rate to 240 Hz, from Equation 2, the limiting MPRT is still 3.33 ms, which is still much longer than that of CRT, which is 1.5 ms.

To achieve a CRT-like MPRT (1.5 ms) for gaming monitors and low latency near-eye displays, low duty ratio (the ratio of emission time to frame time) plays a key role for further suppressing the motion image blurs. When duty ratio is considered, MPRT can be expressed as<sup>74</sup>

$$MPRT \approx 0.8 \times T_f \times DR, \quad (3)$$

where DR is the duty ratio of the display. Let us go back to the 120-Hz display again, where the limiting MPRT ( $0.8T_f$ ) is 6.66 ms. From Equation 3, to obtain  $MPRT = 1.5$  ms, the duty ratio should be kept below 22.5%. Although low duty ratio helps to suppress image blurs, it reduces the display brightness proportionally. To obtain the same brightness, the LED backlight (for LCD) or OLED pixel driving current should be increased. As a result, some trade-offs, such as drooping effect and lifetime, could be compromised.

In LCDs, scanning and blinking backlight is commonly adopted to produce a low duty ratio.<sup>79,80</sup> As the duty ratio decreases, the MPRT is less sensitive to the LC response time. The maximum allowable LC response time  $T_{LC, \max}$  is determined by the frame time, gate scan time ( $T_g$ ), and backlight emission time as follows:

$$T_{LC, \max} = T_f - T_g - T_f \times DR. \quad (4)$$

According to Equations 3 and 4, MPRT decreases almost linearly, and  $T_{LC, \max}$  increases linearly as the duty ratio decreases, as Figure 4 depicts. To leave more time for the LC to respond at a higher frame rate such as 120 Hz, a lower duty ratio should be applied, but the effective transmittance (or display brightness) would be compromised. In order to further clarify the relation between frame rate, LC response time, and duty ratio (effective transmittance), we depict the maximum allowable LC response time and duty ratio as a function of frame rate to achieve 1.5-ms MPRT in Figure 5. A higher frame rate can support a larger duty ratio for achieving a higher effective transmittance; however, a faster LC response time and shorter charging time are required. In other words, a faster LC response time and TFT scan time help to improve the effective transmittance under the same MPRT. Recently, AUO, iBoson, and JDI have demonstrated fast response LCs for high-resolution VR applications.<sup>81,82</sup> The slowest gray-to-gray response time is below 3 ms, and MPRT is 0.9 ms at 90-Hz frame rate, as reported by AUO and iBoson. In parallel, JDI developed a one-side branch structure to realize a fast response time of 2.2 ms for VR displays. To enable a much higher

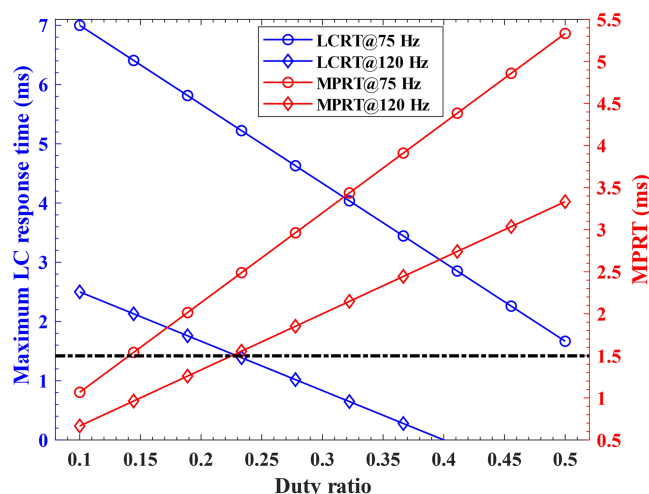
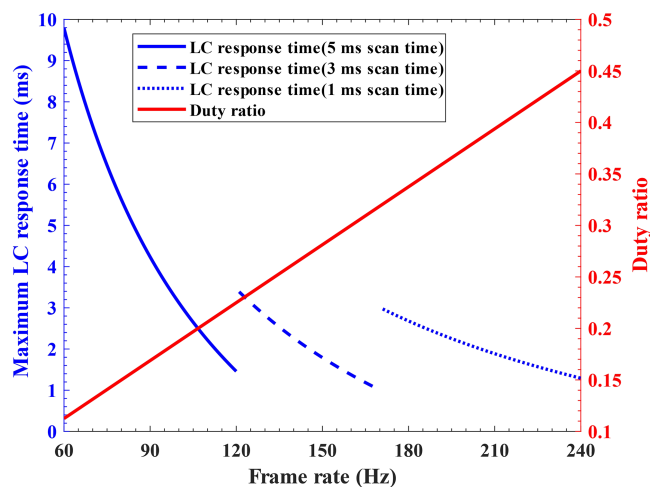


FIGURE 4 Calculated maximum allowable liquid crystal (LC) response time and the corresponding motion picture response time (MPRT) as a function of duty ratio. The gate scan time is assumed to be 5 ms. The black dashed lines represent a cathode ray tube (CRT)-like MPRT = 1.5 ms



**FIGURE 5** Calculated maximum allowable liquid crystal (LC) response time and duty ratio as a function of frame rate to achieve 1.5-ms motion picture response time (MPRT). The gate scan time is assumed to be 5 ms during 60–120 Hz, 3 ms during 120–170 Hz, and 1 ms during 170–240 Hz

frame rate than 120 Hz, the TFT scan time must be further reduced to leave enough time for backlight emission and for the LC to respond. Recently, many efforts are devoted to reducing the charging time.<sup>83,84</sup> It should be mentioned that in Figure 5 when the frame rate is in 170–240 Hz, the scan time is assumed to be 1 ms so that  $T_{LC, \max}$  remains in the 1–3 ms range. However, it is challenging to obtain such a short scan time. A higher frame rate enables a larger duty ratio to achieve the same MPRT, but the electronic power consumption increases.

Analogous to CRT, impulse driving can be applied to LED and OLED devices as well. The major drawback of a low duty ratio is its compromised brightness. For example, if  $DR = 25\%$ , then the display brightness would drop by  $4\times$ . To obtain the same brightness, the driving current for the  $\mu$ LED, OLED, and mLED backlight should increase by  $4\times$ , assuming the operation is in the linear region. However, a too high driving current in mLCD backlight may cause a severe current-resistance drop, which in turn leads to increased power consumption and nonuniform brightness.<sup>85</sup> In OLED devices, the efficiency roll-off and lifetime degradation issues in the high current region should be considered.<sup>86</sup> In  $\mu$ LED displays, the EQE is related to the driving current density. Therefore, designing a duty ratio that allows driving in the peak efficiency region is critical.<sup>87,88</sup>

### 3.3 | Viewing angle

Wide viewing angle is a key requirement for multiviewers display such as TVs and public information

displays. For these applications, the viewers may watch the display from different angles. In addition, for a palm-size smartphone, the user may flip from portrait to landscape mode so that wide viewing angle is also required. However, three important factors should be considered for a wide-view display: decreased CR (e.g., LCDs), angular color shift (all display technologies), and decreased luminance intensity. For LCDs, the gray level of each subpixel is determined by the voltage-dependent LC director reorientation, which modulates the backlight transmittance. When the incident light traverses the birefringent LC layer at different angles, the accumulated phase retardation varies, leading to a different transmittance. For this reason, the voltage-dependent transmittance varies at different viewing directions, giving rise to gamma-curve distortion and color shift.<sup>89,90</sup> The off-axis light leakage from the crossed polarizers worsens the black state, leading to a degraded CR. The off-axis light leakage from the LC depends on the initial LC alignment, for example, it is more severe for VA than for homogeneous alignment. To increase CR and suppress color shift, creating multiple domains and laminating phase compensation films are commonly practiced. For a single-domain TN LCD, Fujifilm has developed a wide-view compensation film to widen its viewing angle.<sup>91</sup> In a VA LCD, multiple domains and compensation films are required for achieving wide view. To create multiple domains, each pixel is divided into several subpixels via patterned electrodes<sup>92</sup> or physical protrusions.<sup>93</sup> Four-domain, eight-domain,<sup>94</sup> and 12-domain<sup>95</sup> VA configurations have been proposed to reduce gamma shift and color washout at large angles. For compensation films, a combination of two A plates and two C plates<sup>96</sup> or a combination of one A plate and one C plate has been proposed to reduce the off-axis light leakage from the VA LC and crossed polarizers. In IPS and FFS modes, the LC directors are aligned homogeneously; thus, with multidomain and phase compensation, a very wide viewing angle and indistinguishable color shift can be achieved. Four-domain LC alignment in the voltage-on state can be provided by zigzag electrodes. Positive A and negative A plates or a pair of positive A and C plates have been employed to suppress the off-axis light leakage from crossed polarizers. To compare the viewing angle of MVA and FFS modes, we simulate their viewing angle with Techwiz LCD 3D. In both modes, Merck negative LC mixture MLC-6608 is used, and zigzag electrodes are employed to realize four-domain LC alignment in the voltage-on state. The physical properties of MLC-6608 are listed as follows:  $\Delta\epsilon = -4.2$  at 1 kHz,  $K_{11} = 16.7$  pN,  $K_{22} = 7.0$  pN,  $\gamma_1 = 186$  mPa·s, and  $\Delta n = 0.083$  at  $\lambda = 550$  nm. The device parameters used in MVA simulation are as

follows: cell gap  $d = 4 \mu\text{m}$ , the width of the chevron-shaped slit is  $w = 6 \mu\text{m}$ , electrode gap  $g = 18 \mu\text{m}$ , and pretilt angle is  $90^\circ$ . The bending angle is  $45^\circ$ , and the compensation films are employed to widen the viewing angle.<sup>97</sup> For the FFS mode, the device parameters used in simulation are as follows: cell gap  $d = 4 \mu\text{m}$ , electrode width is  $w = 3 \mu\text{m}$ , electrode gap  $g = 4.5 \mu\text{m}$ , bending angle =  $10^\circ$ , and pretilt angle =  $2^\circ$ . The simulation results in Figure 6 show that the CR of an LCD decreases as the viewing angle increases, and the FFS mode has a wider viewing angle than the MVA mode owing to its in-plane reorientations of the LC directors.

In an emissive display, the CR does not change according to different viewing angles. However, the angular color shift is still an issue. In an OLED display, two factors are responsible for the angular color shift: microcavity effect and unmatched RGB radiation patterns. As mentioned above, the microcavity is used in OLED devices to boost color purity and optical efficiency. However, as the viewing angle increases, the emission spectrum shifts toward a shorter wavelength due to reduced effective cavity length. Moreover, if the RGB subpixels have unmatched radiation patterns, the RGB light ratio for a mixed color will change, depending on the viewing angle. As a result, a noticeable color shift could occur. The color shift of an OLED display can be mitigated by applying scattering medium inside the cavity, increasing the transmittance of top electrode, optimizing the cavity length of an OLED device structure.<sup>98–102</sup> However, the trade-off in complicated fabrication process,

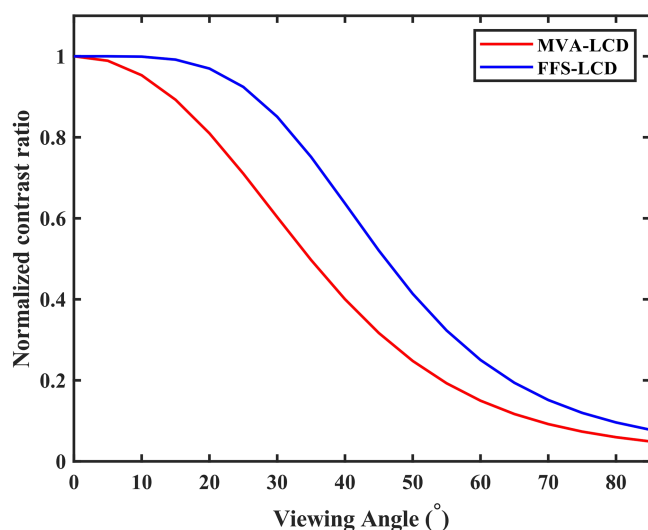


FIGURE 6 Simulated contrast ratio versus viewing angle along the horizontal direction for multidomain vertical alignment (MVA) and fringe-field switching (FFS) liquid crystal displays (LCDs) with four domains

pixel crosstalk, decreased color purity, and EQE drop should be considered.<sup>103–105</sup>

In  $\mu\text{LED}$  displays, the cavity effect is weak, so the central wavelength of RGB subpixels basically remains unchanged regardless of viewing angle.<sup>106</sup> However, a small LED chip size would lead to a nonnegligible sidewall emission,<sup>107–109</sup> and the refractive index difference between red LED and green and blue LEDs results in unmatched RGB radiation patterns. To reduce the unmatched angular radiation patterns between RGB  $\mu\text{LEDs}$ , a specially designed black matrix, LED taper angle, and optical structure have been proposed,<sup>106,109,110</sup> but the trade-off in light extraction efficiency should be considered.

To quantitatively evaluate the viewing angle performance for LCD, OLED, and  $\mu\text{LED}$ , iPhone 11 (LCD screen), iPhone 11 Pro Max (OLED screen), and  $\mu\text{LED}$  reported by Sony<sup>110</sup> are selected for comparison. For iPhone 11 and iPhone 11 Pro Max, the color shift is calculated from measured spectrum at different angles, and the luminous intensity is measured by the RiGO801 Goniophotometer (TechnoTeam Vision). For  $\mu\text{LED}$ , the color shift of white light is calculated according to the angular intensity distribution for three RGB primaries, and the luminous intensity for white light is close to Lambertian distribution. Figure 7A shows that iPhone 11 Pro Max (OLED display) has the largest angular color shift at  $60^\circ$  due to the blue shift effect of the microcavity. For the  $\mu\text{LED}$  display, its luminous intensity for the red primary and blue primary has the biggest mismatch at  $60^\circ$ , leading to a dramatically increased color shift. In the FFS LCD, the voltage-dependent transmittance for the RGB primaries varies with viewing angle, giving rise to the color shift shown in Figure 7A. It should be mentioned that if  $\Delta u'v' < 0.02$ , the color shift remains indistinguishable by human eye. The angular distribution for LCD, OLED, and  $\mu\text{LED}$  can be tailored according to a specific application. For example, a wide angular distribution is desired for TV applications due to multiple observers; however, it can be narrowed down to increase the on-axis luminance for mobile devices. Functional optical films such as brightness enhancement films can be employed in the LCD backlight system to control the angular distributions. Microcavities and nanostructures can be applied to tailor the angular distributions of an OLED display.<sup>102</sup> Finally, optical structures such as shaped sidewalls and microlens arrays are used to tailor the angular distributions of a  $\mu\text{LED}$  display, for example, InfiniLED reported parabolic reflective sidewalls for collimating the light emitted from  $\mu\text{LEDs}$ .<sup>111</sup> Figure 7B depicts the angular distributions of three commercial products we evaluated: iPhone 11 (LCD screen), iPhone 11 Pro Max (OLED screen), and  $\mu\text{LED}$ .<sup>110</sup>



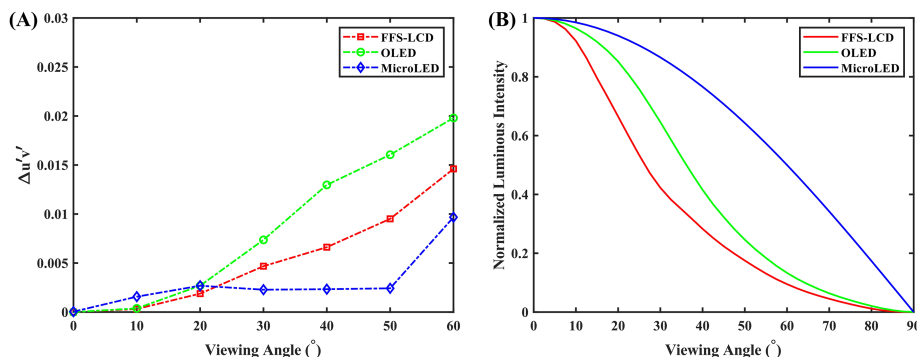


**FIGURE 7** (A) Color shift for white light versus viewing angle in the horizontal direction. (B) Normalized luminous intensity for white light versus viewing angle along horizontal direction. The color shift and angular distribution of fringe-field switching (FFS) liquid crystal display (LCD) and organic light-emitting diode (OLED) display are measured from iPhone 11 and iPhone 11 Pro Max, respectively. For the micro-light-emitting diode ( $\mu$ LED) display, results are replotted from Biwa et al.<sup>110</sup>

### 3.4 | Color gamut

Vivid color is another desirable requirement for display devices. Before comparing the color performance of these three display technologies, let us first discuss the relation between color gamut and luminous efficacy of radiation (LER).<sup>112</sup> LER is a metric for evaluating the conversion of the emitted display radiation flux into the luminous flux perception of human eye. It is defined as

$$LER = \frac{683 \times \int P_{display}(\lambda) V(\lambda) d\lambda}{\int P_{display}(\lambda) d\lambda}, \quad (5)$$

where  $V(\lambda)$  is the human eye sensitivity function. The maximum value of LER is 683 lm/W for a monochromatic light source at  $\lambda = 555$  nm. According to the human eye sensitivity function, as the wavelength of light moves away from 555 nm, the luminance efficiency will decrease. Thus, although a deeper red or blue color helps widen the color gamut, it also lowers the overall luminance efficiency. Therefore, the subtle trade-off between LER and color gamut should be taken into consideration.

By varying the central wavelength and full width at half maximum (FWHM) of RGB spectra, all optimized solutions are located on the Pareto front, shown in Figure 8. Generally, there is an obvious trade-off between LER and color gamut: as the color gamut increases, LER declines. The details depend on the FWHM. At a given color gamut, say 80% Rec.2020, narrowing the FWHM from 50 to 10 nm helps to increase LER, but the gain gradually saturates. Although wider color gamut results in a lower LER, according to the Helmholtz–Kohlrausch (HK) effect,<sup>113</sup> the perceived image is brighter for the display with a wider color gamut (more saturated color). Based on the display quality score,<sup>114</sup> the display quality is affected by both luminance and color area. A wider color gamut display can achieve the same image quality

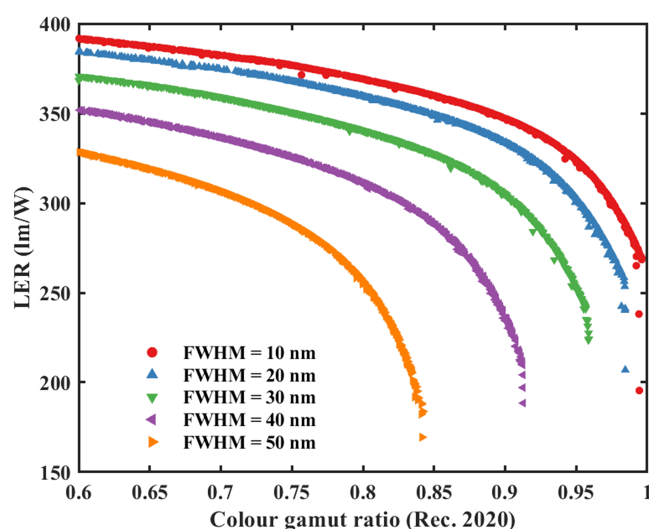


**FIGURE 8** Pareto front defined in International Commission on Illumination (CIE) 1931 with different full width at half maximum (FWHM) light sources

with a lower luminance.<sup>115</sup> Thus, a delicate balance between color gamut and efficiency should be carefully considered in practical applications.

For LCDs, the color conversion materials have been improved from yellow YAG phosphor, two-color phosphors (green:  $\beta$ -sialon:  $\text{Eu}^{2+}$  phosphor; red: KSF phosphor), to quantum dots (QDs) or perovskites.<sup>116</sup> The corresponding color gamut is expanded from  $\sim 50\%$ ,  $\sim 70\%$ , to  $\sim 90\%$  Rec.2020. In an LCD, the blue LED-converted white light is further filtered by the RGB color filters to generate three primary colors. However, because the RGB transmission bands of the pigment-based color filters are relatively broad and do not completely match the emission spectra from the LCD backlight, crosstalk is appreciable especially in the blue-green and orange-yellow regions. A narrow band color filter helps to reduce the crosstalk and increase the color gamut to about 90%

Rec.2020, but its larger absorption reduces the optical efficiency.<sup>117</sup>

Both OLED and  $\mu$ LED are emissive displays. Their color gamut mainly depends on the emission spectrum of the RGB emitters. Among OLED displays, deep blue fluorescent and deep red phosphorescent OLEDs have recently been released. As a result, their color gamut can also achieve over 90% Rec.2020.<sup>115,118</sup> In a  $\mu$ LED display, the emission spectrum is mainly defined by the band structure of MQWs. The FWHM of red and blue emission spectra is usually below 20 nm, but the green is broader, as Figure 4C depicts. Green LEDs also suffer from efficiency lag, which is commonly known as “green gap.”<sup>119</sup> Moreover, the color performance of an LED display is affected by the center wavelength shift under different driving currents.<sup>120</sup> Generally, as the driving current increases, the central wavelength of the LED will blue-shift due to the quantum-confined Stark effect and then redshift due to an increased junction temperature. To solve the wavelength shifting problem in an  $\mu$ LED display, the pulse width modulation (PWM)<sup>121</sup> driving method that drives with a fixed current and modulates the grayscale by the LED emission time is commonly adopted. However, it is challenging for PWM to achieve a short emission time in low gray levels, especially at a high frame rate. Therefore, a hybrid (digital and analog) driving method for  $\mu$ LED displays has also been proposed.<sup>122</sup>

By adding color conversion materials such as QDs or perovskite on top of the emission source (blue OLED or  $\mu$ LED), full colors can also be achieved. According to the emission spectrum of the color conversion material with an ultranarrow FWHM, a color gamut greater than 95% Rec.2020 can be achieved in theory.<sup>123–126</sup> However, some key issues remain to be solved, for example, blue light leakage would reduce the color purity of the display, the power conversion efficiency of the color conversion layer, and the ambient light excitation of the color conversion layer placed at top of the display panel.<sup>127–129</sup>

When comparing different display technologies, three typical light source spectra for QD-LCD, OLED, and  $\mu$ LED are plotted in Figure 9.<sup>117,130,131</sup> Figure 10 shows their color gamut in Rec.2020 color space. For the QD-LCD with commercial color filters, its color gamut is  $\sim$ 84% Rec.2020, which is limited by the crosstalk of the color filters. For the RGB  $\mu$ LED display, because of the relatively broad green  $\mu$ LED spectrum ( $\sim$ 40 nm), the

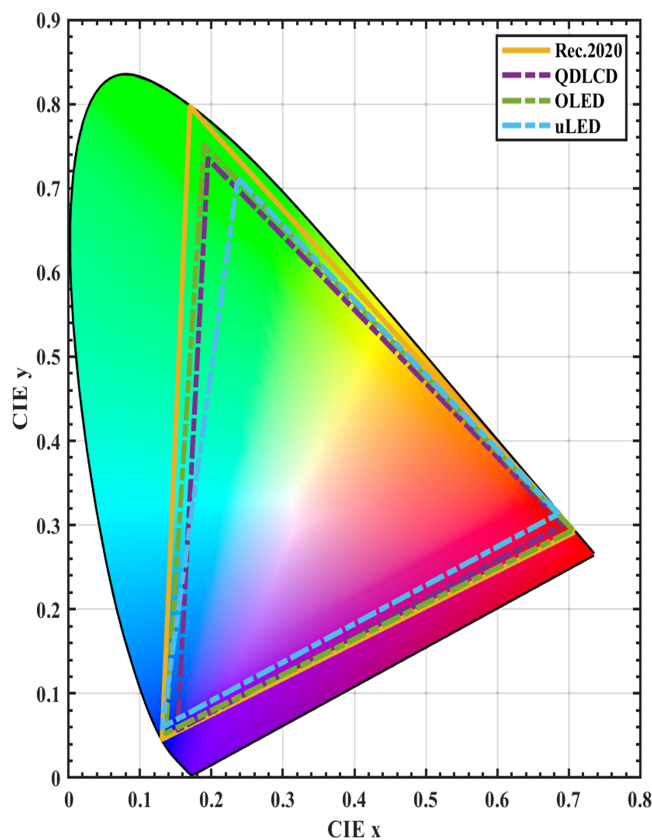


**FIGURE 10** Chromaticity ( $x, y$ ) of liquid crystal display (LCD), micro-light-emitting diode ( $\mu$ LED), and organic light-emitting diode (OLED) displays in comparison with Rec.2020 in International Commission on Illumination (CIE) 1931 color space

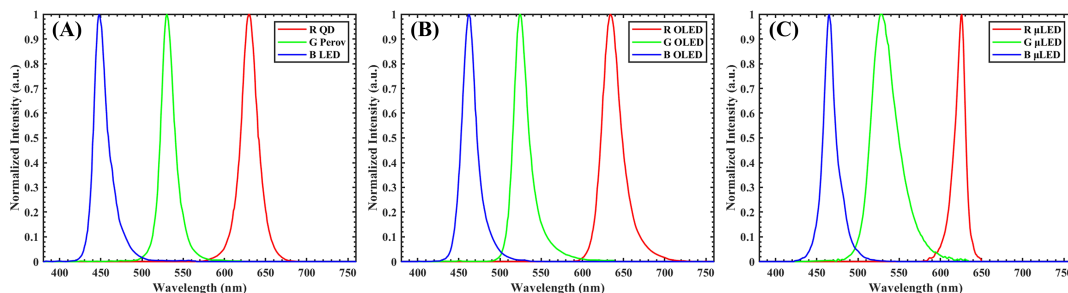


**FIGURE 9** (A) Quantum dot liquid crystal display (QD-LCD), (B) organic light-emitting diode (OLED), and (C) micro-light-emitting diode ( $\mu$ LED) light source spectra

green point deviates noticeably in Rec.2020 color space so that its color gamut is also  $\sim 80\%$ . Finally, the RGB OLED display with optimized cavity effects can achieve  $\sim 90\%$  Rec.2020 in International Commission on Illumination (CIE) 1931.

In addition, because color space is three dimensional, the CIELAB standard, which has good homogeneity in the color space, is recommended by CIE to present the color performance of display devices. Therefore, we also calculate the Rec.2020 volume-coverage ratio in color appearance model CIELAB, as shown in Figure 11. The calculated volume-coverage ratio is also noted.

The above display performance is obtained in a laboratory environment, but in commercial products, more issues need to be considered. For example, in mobile devices, QD enhancement film (QDEF) is not used because of its increased thickness. Therefore, phosphor-based white LEDs are still the mainstream approach for the backlight source. Here, we summarize the color performance comparison of two commercial mobile devices: RGB OLED in iPhone 11 Pro Max and LCD (KSF white LED backlight) in iPhone 11, their color gamut coverage is about 97% DCI-P3 (74% Rec.2020) and 96% DCI-P3 (70% Rec.2020) in the CIE 1931 color space. In iPhone 12, the color gamut of OLED panel is almost the same as that of iPhone 11 Pro Max. In mobile displays, the DCI-P3 color standard usually supports most image contents. Therefore, further widening the color gamut is not their top priority.

For nonportable display applications such as monitors and TVs, even if QDEF can be applied, the European Union has passed Restriction of Hazardous Substances (RoHS) to limit the maximum cadmium concentration to 100 ppm in electrical and electronic equipment. Since 2015, Samsung has greatly improved the optical performance of InP-based QD materials that comply with RoHS regulations. Recently, they have increased the color coverage of InP-based QDEF LCD panels to 71.2% Rec.2020

in the CIE 1931 color space.<sup>132</sup> Compared with the cadmium-based QDEF that can cover more than 80% Rec.2020 in the 1931 color space, there is still room for improvement.

### 3.5 | ACR-based power consumption model

Low power consumption is highly desirable because limited battery capacity governs the operation time of the mobile display devices. Although TVs and monitors are powered by the wall plugs, low power consumption helps to save the ecosystem. For a long time, the power efficiency of the display panel has been merely determined by the optical efficiency (EQE or wall-plug efficiency) of the emission source (LED/OLED) and the transmittance of the display panel. However, in these power consumption models, the influence of ambient reflectance is not taken into consideration.<sup>133</sup> Especially, when the ambient light is strong, the reflected ambient light could washout the displayed image. Under such condition, boosting display brightness is a viable solution. Recently, a power consumption model based on ACR has been proposed.<sup>134</sup> The power consumption of displays is compared under the same ACR. Based on Equation 1, the on-axis display brightness for providing the targeted ACR under different ambient light level can be described by

$$L_{on} = ACR \times L_{off} + (ACR - 1) \times L_{ambient} \times R, \quad (6)$$

where  $L_{on}$  ( $L_{off} \approx 0$  for emissive display) represents the on (off)-state luminance of the display,  $L_{ambient}$  is the ambient luminance, and  $R$  is the ambient light reflectance depending on the display technologies. Here, white image with color coordinate  $CIE_x = 0.312$ ,  $CIE_y = 0.329$  is used as standard to compare the power consumption of various display technologies. The corresponding

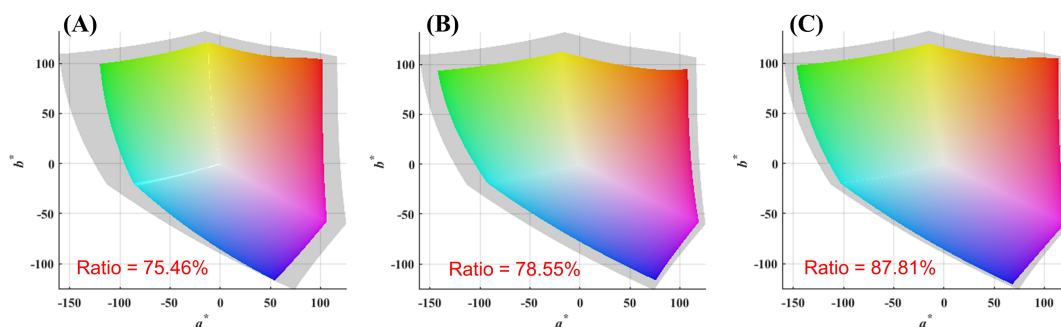


**FIGURE 11** Color gamut comparison in Rec.2020 for (A) light-emitting diode (LED), (B) quantum dot liquid crystal display (QD-LCD), and (C) organic light-emitting diode (OLED) display in CIELAB. The gray color gamut is Rec.2020, and the solid color gamut is the target display

brightness of three RGB primary colors is determined by color mixing principle. Then, the total luminous flux from the emission source can be calculated by

$$\Phi_{RGB} = L_{RGB} \int_0^{2\pi} d\phi \int_0^{\alpha} f_{RGB}(\theta) \sin \theta d\theta \times A_p / T_{sys}, \quad (7)$$

where  $\Phi$  is the luminous flux,  $L$  is the on-axis brightness,  $\alpha$  is half of the viewing angle,  $f(\theta)$  is the angular distribution,  $A_p$  is the pixel size, and  $T_{sys}$  is the transmittance of the display system.

In addition, based on the luminance efficacy ( $K$ ), average photon energy ( $h\nu$ ), and EQE of the emission devices, the power efficiency (lm/W) can be derived as

$$\eta_{RGB} = \frac{EQE_{RGB} \times K_{RGB} \times h\nu_{RGB}}{q \times V_{RGB}}, \quad (8)$$

where  $V$  is the driving voltage and  $q$  is the elementary charge. From Equations 7 and 8, the display power consumption is the ratio of total display luminous flux to the power efficiency.

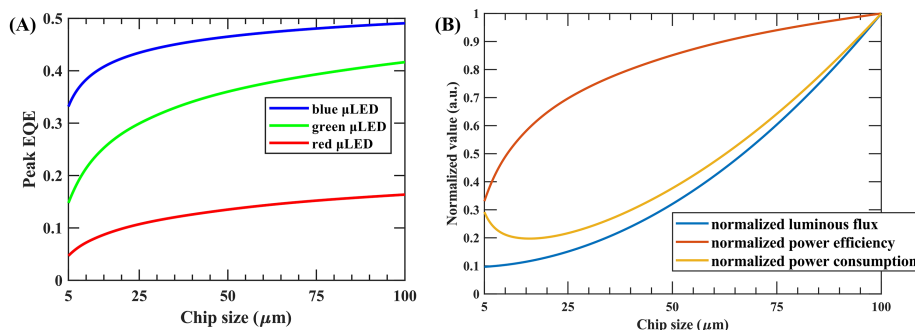
Overall, due to the nonradiative recombination at the etched sidewalls, the peak EQE decreases as the  $\mu$ LED chip size decreases. As discussed in previous studies,<sup>135–137</sup> the phenomenon is more pronounced as the chip size is less than 100  $\mu\text{m}$ . In addition, because the surface recombination velocity of AlGaInP is higher than that of InGaN, the efficiency drop of red  $\mu$ LED is more serious than the blue and green ones as the chip size decreases.<sup>138</sup> The peak EQE of RGB LEDs as a function of chip size is plotted in Figure 12A.<sup>139,140</sup>

Based on Equation 8, a larger LED chip size with higher EQE is helpful to enhance the power efficiency. However, as discussed above, the larger LED chip size results in a stronger ambient luminous reflectance so that a higher luminance is required to maintain the same ACR. Based on the trade-off between display ambient reflectance and power efficiency, the optimal LED chip

size with minimum power consumption can be found. Here, three kinds of display applications under specific ambient condition are analyzed: (1) smartphone (PPI [pixel per inch] = 460) under 2000-lux overcast daylight for ACR = 30:1, (2) laptop (PPI = 280) under 450-lux office light for ACR = 120, and (3) TV (PPI = 68) under 200-lux living room light for ACR = 800. Let us firstly focus on the TV applications. From Equations 6 and 7, the total luminous flux of display as function of LED chip size is defined as  $\Phi(x)$  and plotted by blue color in Figure 12B. As the LED chip size increases, the higher ambient reflectance demands a higher luminous flux to keep the same ACR. On the other hand, from Equation 8, the power efficiency as a function of LED chip size is defined as  $P(x)$  and plotted by orange color in Figure 12B. The larger LED chip size brings out higher EQE and power efficiency. Then, the optimal LED chip size with minimum power consumption can be found when the ratio of  $\Phi(x)$  over  $P(x)$  has a minimum, as plotted in yellow color in Figure 12B. Compared with the 100- and 5- $\mu\text{m}$  chip sizes, the optimal LED chip size (16  $\mu\text{m}$ ) can save 40% and 32% power consumption, respectively. These results manifest the advantage of using optimized LED chip size. Following the same analysis process, we find the optimal LED chip size for smartphone is 6  $\mu\text{m}$  and for laptop is 8  $\mu\text{m}$ .

In addition, because the RGB LEDs have different power efficiency declining rate, ambient reflectance, and the color mixing ratio, these varieties provide the flexibility to further reduce overall power consumption by applying RGB LED with nonuniform chip sizes. By lifting the restrictions on  $\mu$ LED chip sizes, a systematic optimization is conducted to achieve the lowest power consumption. The optimal chip size in RGB subpixels is (10, 5, 5)  $\mu\text{m}$  for the smartphone, (14, 7, 5)  $\mu\text{m}$  for the laptop, and (26, 13, 8)  $\mu\text{m}$  for the TV studied. The power saving between two  $\mu$ LED displays with different chip sizes and with uniform chip size in DCI-P3 color space is plotted in Figure 13. Overall, the power saving covers over 90% of DCI-P3 color space. It is worth noting that the power

**FIGURE 12** (A) Chip size dependent peak external quantum efficiency (EQE) of red, green, and blue (RGB) micro-light-emitting diodes ( $\mu$ LEDs). (B) Normalized power efficiency fitting function (orange line), normalized luminous flux (blue line), and normalized power consumption function (yellow line)





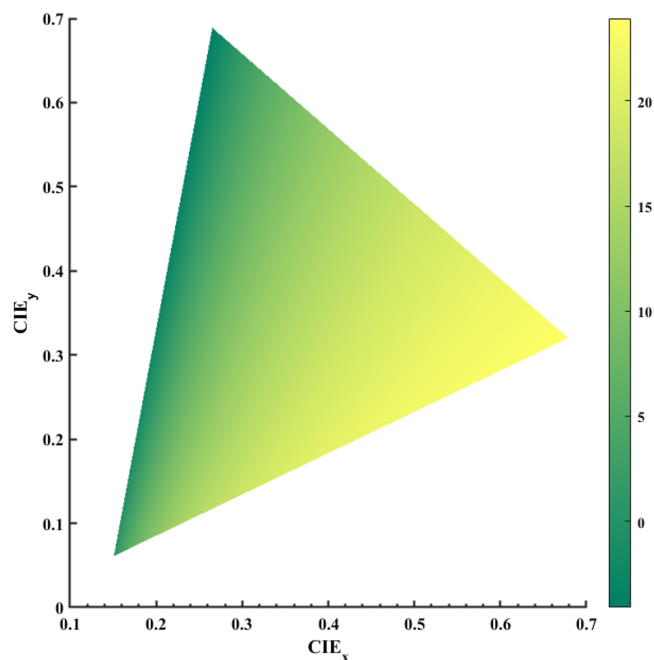


**FIGURE 13** The power saving (unit: %) between red, green, and blue (RGB) micro-light-emitting diode ( $\mu$ LED) displays with different chip sizes and uniform chip size

saving is image dependent and the maximum power saving (>20%) occurs at red color. In addition, for the standard white image D-65, the power saving is about 15%.

The power efficiency of an OLED, which is governed by the IQE and light extraction efficiency (LEE) of the OLED device, has been significantly improved in the past few years. As mentioned above, the IQE of second-generation OLED materials with phosphorescent emitters have already reached 100%, so extensive research efforts are devoted to increasing the light extraction efficiency of the OLEDs. Normally, only 20% of the emitting light can be extracted out. Other emitting light is either guided in substrate, OLED layers, or lost by the surface plasmons in the organic/metal surface. Microlens arrays, high index substrates, and embedded photonic nanostructures can help extract light from OLED devices.<sup>141–145</sup> However, because of complicated manufacture processes, image blur, and haze, these light extraction techniques have not been practiced.<sup>146–148</sup> Recently, 3D pixel configuration of OLED with simulated LEE of  $\sim$ 80% has been proposed. The sidewall reflector in the filler redirects the total internal reflection (TIR) rays to out-coupling through one or multiple reflections.<sup>148</sup>

For LCDs, the polarizer absorbed  $\sim$ 50% of the back-light. To enhance optical efficiency, a dual brightness enhancement film is commonly embedded to recycle the mismatched polarization and boost the efficiency by  $\sim$ 60%.<sup>149</sup>

Generally, self-emissive displays (OLED and  $\mu$ LED) should be more efficient than LCDs when displaying dark images because most pixels are turned off. However, the local dimming method significantly improves the power efficiency of mLCD in low APL images.<sup>150</sup> Next, let us discuss the power efficiency of OLED and  $\mu$ LED displays. First, the phosphorescence green and red OLEDs have  $\sim$ 100% efficiency and blue OLED has 62.5%. However, OLED panels require a circular polarizer to keep a high ACR. Such a circular polarizer not only absorbs  $\sim$ 50% of the emitted OLED light but also increases the panel thickness, which reduces the panel's flexibility. In addition, as discussed above, most optical structures that enhance the LEE of OLED panels introduce side effects and thus are not yet implemented in commercial products. On the other hand, a  $\mu$ LED display with small aperture ratio ( $\sim$ 1%) does not require a circular polarizer. However, until now, the EQE of GaN  $\mu$ LEDs is mostly limited to 10% to 30%,<sup>151,152</sup> which is much lower than the target EQE (80%) for LED lighting. As all technologies continue to advance, the competition results on power consumption will undoubtedly keep changing over time.

### 3.6 | Resolution density

The required display resolution depends on the viewing distance and field of view. So far, in most display applications, such as TVs and desktop monitors, the resolution is adequate due to the relatively long viewing distance. However, in AR/VR displays, the viewing distance is short. To avoid the screen-door effect, a resolution density over 2000 PPI is required. In addition, the light field display that usually loses half of the resolution for generating 3D images requires a high-resolution display. The resolution density of an LCD is determined by the TFT and driving circuit arrangement. In 2017, by new pixel design (staggered octagon) and small-size TFT, Samsung demonstrated an LCD with 2250 PPI.<sup>153</sup> Besides, field sequential color is an elegant approach to triple the resolution density of an LCD. However, the frame rate should exceed 360 Hz to mitigate the color breakup.<sup>154–156</sup> The pixel density of an RGB OLED display is restricted by the shadowing effect when depositing the material through a fine metal mask. Therefore, a well-defined color filter array is widely applied to white OLED emitter to achieve a PPI over 3000.<sup>157</sup> To avoid the absorption loss from color filters, eMagin proposed a novel direct patterning approach and demonstrated an RGB OLED with 2645 PPI. By removing the color filters, both maximum brightness and power efficiency can be improved.<sup>158</sup> Recently, an OLED microdisplay with more

than 10,000 PPI has been proposed,<sup>159</sup> the spatially distributed metasurfaces with different reflection phase is designed in the microcavity to tune the cavity resonances in RGB subpixels. In parallel,  $\mu$ LED microdisplays with PPI > 5000 have also been developed.<sup>160,161</sup> In comparison with OLED,  $\mu$ LED has advantages in high peak luminance<sup>162</sup> and long lifetime. Thus, it is more suitable for AR applications. However, how to achieve full color is still a bottleneck.

### 3.7 | Cost

Cost is often a decisive factor for consumers to purchase a display product. Active-matrix LCDs have been developed since 1980s. Nowadays, the cost of LCDs is reasonably affordable. However, if the mini-LED backlight is implemented, the number of LED chips would increase from few hundreds to tens of thousands. As a result, based on a market analysis,<sup>163</sup> the cost of mLCD has risen by  $\sim 5\times$ , approaching to its OLED counterpart with the same screen size and resolution. However, as the mini-LED backlight technology matures, its cost should drop gradually so that its competitiveness will increase substantially. Similarly, after over 30 years of active development, OLED technology is also reasonably mature, especially for small-sized displays. The manufacturing yield has been greatly improved. With continuous innovations in materials and device structures, and advanced manufacturing processes, such as inkjet printing, OLED's cost should also continue to decline. As for  $\mu$ LED displays, their cost is related to the chip size. Minimizing LED chip size helps increase the number of chips per wafer, but the mass transfer yield could be compromised.

A lower mass transfer yield would lead to a higher repair cost and longer lead time.<sup>53</sup> In addition, smaller chip size also causes more material waste during chip singulation process.

### 3.8 | Lifetime

Both LCD and  $\mu$ LED displays use inorganic materials as backlight and emitting light sources. Their lifetime can easily exceed 50,000 h. However, the light-emitting layer of an OLED display is organic material which is more sensitive to moisture, air, heat, and DC current. Therefore, a special protective film is needed to prevent it from environmental damage.<sup>164</sup> In addition, the differential aging between three primary colors and image sticking effects (also known as burn-in) still need improvement.<sup>165,166</sup> Generally, for red and green ph-OLEDs, their lifetime ( $T_{50}$ ) under 1000 nits is longer than 80,000 h. However, the lifetime of blue phosphorescent OLED is around  $20\times$  shorter than that of red and green ones.<sup>167,168</sup>

Recently, several new materials and novel device structures have been proposed.<sup>169,170</sup> The lifetime of OLED displays is expected to be improved continuously.

### 3.9 | Panel flexibility

Flexibility is a desirable feature for some display applications, such as vehicle displays, smart watches, smartphones (Galaxy S series and Z Flip), and even TVs (LG rollable OLED). Due to excellent flexibility of organic materials, rollable AMOLED displays have been released commercially. The development of ultrathin

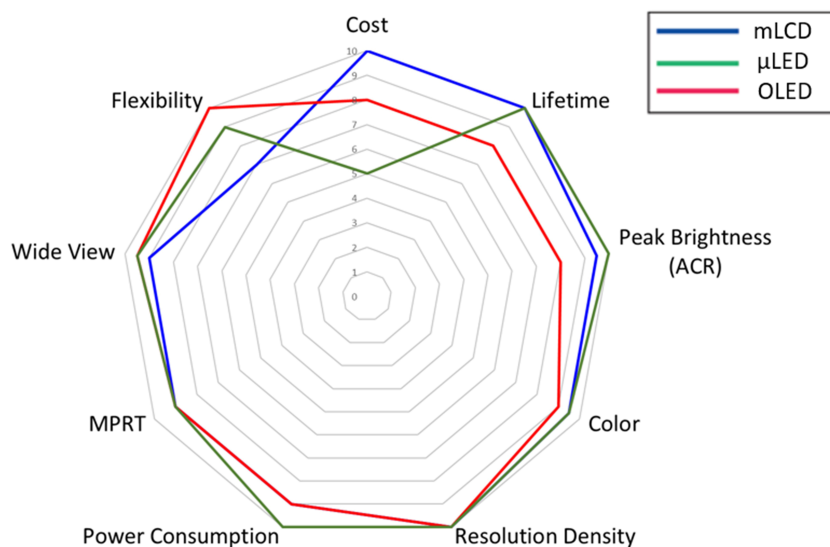


**FIGURE 14** Display performance metrics comparison between mini-light-emitting diode (LED) backlit liquid crystal display (mLCD), red, green, and blue (RGB) organic light-emitting diode (OLED), and RGB micro-LED displays

polarizers<sup>171</sup> and the electrodes with large strain stretchability<sup>172</sup> are key factors to maintain the image quality and tenacity of flexible OLED displays. A flexible transparent  $\mu$ LED display on a polyimide substrate is demonstrated by PlayNitride.<sup>131</sup> For LCDs, a backlight unit is required so that its flexibility is limited. About 5 years ago, FlexEnable demonstrated a rollable LCD using organic TFTs, called OLCD.<sup>173</sup> To keep the LC cell gap uniform during bending, polymer walls are implemented. For a transmissive OLCD, flexible backlight is required.<sup>174</sup> If continuous flexibility is not absolutely required, a foldable LCD can be realized by the tiling two or more borderless LCDs together. At Touch Taiwan 2019, Innolux demonstrated an impressive threefold splicing display with three nearly borderless LCD panels.

## 4 | CONCLUSION

We have briefly reviewed the latest developments in mLCD, OLED, and  $\mu$ LED displays. Each technology has its own pros and cons. We summarize the nine display performance metrics in Figure 14. Overall, the lifetime of OLED displays remains to be overcome for high-brightness applications, such as sunlight readable displays. The relatively low CR degrades the image quality of LCDs at dark ambient. However, considering the ambient light effect, LCD can have a higher ACR than OLED display because of its higher peak brightness. As HDR display becomes mainstream, the competition between OLED and mini-LED will further intensify. Finally,  $\mu$ LED displays show an excellent ACR in almost all ambient conditions, thanks to its high peak brightness. However, the complex driving circuitry and manufacturing process still impede its widespread applications. As the cost continues to decline,  $\mu$ LED displays will gradually move toward the center stage.

## ACKNOWLEDGMENTS

The UCF group is indebted to a.u.Vista, Inc. (65018A64) for the financial support, Jason Adams for useful discussion, and TechnoTeam Vision for sharing the Goniophotometer.

## ORCID

Zhiyong Yang  <https://orcid.org/0000-0002-7181-7443>

Shin-Tson Wu  <https://orcid.org/0000-0002-0943-0440>

## REFERENCES

- Schadt M. Milestone in the history of field-effect liquid crystal displays and materials. *Jpn J Appl Phys.* 2009;48:03B001.
- Tang CW, VanSlyke SA. Organic electroluminescent diodes. *Appl Phys Lett.* 1987;51(12):913–915.
- Jiang HX, Jin SX, Li J, Shakya J, Lin JY. III-nitride blue microdisplays. *Appl Phys Lett.* 2001;78(9):1303–1305.
- Lin JY, Jiang HX. Development of microLED. *Appl Phys Lett.* 2020;116(10):100502.
- Yeh P, Gu C. *Optics of Liquid Crystal Displays.* John Wiley & Sons; 2009.
- Yang DK, Wu ST. *Fundamentals of Liquid Crystal Devices.* John Wiley & Sons; 2014.
- Chen HW, Lee JH, Lin BY, Chen S, Wu ST. Liquid crystal display and organic light-emitting diode display: present status and future perspectives. *Light Sci Appl.* 2018;7(3):17168.
- Tsujimura T. *OLED Display Fundamentals and Applications.* John Wiley & Sons; 2017.
- Geffroy B, Le Roy P, Prat C. Organic light-emitting diode (OLED) technology: materials, devices and display technologies. *Polym Int.* 2006;55(6):572–582.
- Huang Y, Hsiang EL, Deng MY, Wu ST. Mini-LED, micro-LED and OLED displays: present status and future perspectives. *Light Sci Appl.* 2020;9(1):105.
- Tian P, McKendry JJ, Gong Z, et al. Size-dependent efficiency and efficiency droop of blue InGaN micro-light emitting diodes. *Appl Phys Lett.* 2012;101(23):231110.
- Jiang HX, Lin JY. Nitride micro-LEDs and beyond—a decade progress review. *Opt Express.* 2013;21(103):A475–84.
- Liu Z, Lin CH, Hyun BR, et al. Micro-light-emitting diodes with quantum dots in display technology. *Light Sci Appl.* 2020;9(1):83.
- Li Y, Chu P, Liu J, Du S. A novel partitioned light guide backlight LCD for mobile devices and local dimming method with nonuniform backlight compensation. *J Display Technol.* 2014;10(4):321–328.
- Yoon GW, Bae SW, Lee YB, Yoon JB. Edge-lit LCD backlight unit for 2D local dimming. *Opt Express.* 2018;26(16):20802–20812.
- Tan G, Huang Y, Chen MC, Lee SL, Wu ST. High dynamic range liquid crystal displays with a mini-LED backlight. *Opt Express.* 2018;26(13):16572–16584.
- Zheng B, Deng Z, Zheng J, et al. 41-2: Invited Paper: An advanced high-dynamic-range LCD for smartphones. *SID Symp Dig Tech Pap.* 2019;50(1):566–568.
- Hsiang EL, Yang Q, He Z, Zou J, Wu ST. Halo effect in high-dynamic-range mini-LED backlit LCDs. *Opt Express.* 2020;28(24):36822–36837.
- Lin FC, Huang YP, Liao LY, et al. Dynamic backlight gamma on high dynamic range LCD TVs. *J Disp Technol.* 2008;4(2):139–146.
- Chen H, Zhu R, Li MC, Lee SL, Wu ST. Pixel-by-pixel local dimming for high-dynamic-range liquid crystal displays. *Opt Express.* 2017;25(3):1973–1984.
- Guarnieri G, Albani L, Ramponi G. Minimum-error splitting algorithm for a dual layer LCD display—part II: implementation and results. *J Disp Technol.* 2008;4(4):391–397.
- Jin L, Yang Z, Liu H, et al. Color moiré of a high dynamic range dual-panel LCD. *OSA Contin.* 2020;3(5):1105–1116.
- Schadt M, Helfrich W. Voltage-dependent optical activity of a twisted nematic liquid crystal. *Appl Phys Lett.* 1971;18(4):127–128.

24. Schiekel MF, Fahrenschon K. Deformation of nematic liquid crystals with vertical orientation in electrical fields. *Appl Phys Lett*. 1971;19(10):391–393.
25. Soref RA. Transverse field effects in nematic liquid crystals. *Appl Phys Lett*. 1973;22(4):165–166.
26. Lee SH, Lee SL, Kim HY. Electro-optic characteristics and switching principle of a nematic liquid crystal cell controlled by fringe-field switching. *Appl Phys Lett*. 1998;73(20):2881–2883.
27. Kim SS, You BH, Cho JH, Kim DG, Berkeley BH, Kim ND. An 82-in. ultra-definition 120-Hz LCD TV using new driving scheme and advanced Super PVA technology. *J Soc Inf Disp*. 2009;17(2):71–78.
28. Lee SH, Kim SM, Wu ST. Review paper: Emerging vertical-alignment liquid-crystal technology associated with surface modification using UV-curable monomer. *J Soc Inf Disp*. 2009;17(7):551–559.
29. Choi TH, Woo JH, Choi Y, Yoon TH. Interdigitated pixel electrodes with alternating tilts for fast fringe-field switching of liquid crystals. *Opt Express*. 2016;24(24):27569–27576.
30. Yu IH, Song IS, Lee JY, Lee SH. Intensifying the density of a horizontal electric field to improve light efficiency in a fringe-field switching liquid crystal display. *J Phys D Appl Phys*. 2006;39(11):2367–2372.
31. Ge Z, Wu ST, Kim SS, Park JW, Lee SH. Thin cell fringe-field-switching liquid crystal display with a chiral dopant. *Appl Phys Lett*. 2008;92(18):181109.
32. Kim DH, Lim YJ, Kim DE, Ren H, Ahn SH, Lee SH. Past, present, and future of fringe-field switching-liquid crystal display. *J Soc Inf Disp*. 2014;15(2):99–106.
33. Chen H, Gao Y, Wu ST. 49.1: Invited Paper: n-FFS vs. p-FFS: who wins? *SID Symp Dig Tech Pap*. 2015;46(1):735–738.
34. Chen H, Peng F, Hu M, Wu ST. Flexoelectric effect and human eye perception on the image flickering of a liquid crystal display. *Liq Cryst*. 2015;42(12):1730–1737.
35. Kim S, Kwon HJ, Lee S, et al. Low-power flexible organic light-emitting diode display device. *Adv Mater*. 2011;23(31):3511–3516.
36. Chen SF, Wang CW. Influence of the hole injection layer on the luminescent performance of organic light-emitting diodes. *Appl Phys Lett*. 2004;85(5):765–767.
37. Takada N, Tsutsui T, Saito S. Control of emission characteristics in organic thin-film electroluminescent diodes using an optical-microcavity structure. *Appl Phys Lett*. 1993;63(15):2032–2034.
38. Thomschke M, Nitsche R, Furno M, Leo K. Optimized efficiency and angular emission characteristics of white top-emitting organic electroluminescent diodes. *Appl Phys Lett*. 2009;94(8):59.
39. Riel H, Karg S, Beierlein T, Rieß W, Neyts K. Tuning the emission characteristics of top-emitting organic light-emitting devices by means of a dielectric capping layer: an experimental and theoretical study. *J Appl Phys*. 2003;94(8):5290–5296.
40. Hung LS, Tang CW, Mason MG, Raychaudhuri P, Madathil J. Application of an ultrathin LiF/Al bilayer in organic surface-emitting diodes. *Appl Phys Lett*. 2001;78(4):544–546.
41. Riel H, Karg S, Beierlein T, Ruhstaller B, Rieß W. Phosphorescent top-emitting organic light-emitting devices with improved light outcoupling. *Appl Phys Lett*. 2003;82(3):466–468.
42. Chwang AB, Rothman MA, Mao SY, et al. Thin film encapsulated flexible organic electroluminescent displays. *Appl Phys Lett*. 2003;83(3):413–415.
43. Kondakov DY. Characterization of triplet-triplet annihilation in organic light-emitting diodes based on anthracene derivatives. *J Appl Phys*. 2007;102(11):114504.
44. Baldo M, Lamansky S, Burrows P, Thompson M, Forrest S. Very high-efficiency green organic light-emitting devices based on electrophosphorescence. *Appl Phys Lett*. 1999;75(1):4–6.
45. Nakanotani H, Higuchi T, Furukawa T, et al. High-efficiency organic light-emitting diodes with fluorescent emitters. *Nat Commun*. 2014;5(1):1–7.
46. Park YS, Lee S, Kim KH, Kim SY, Lee JH, Kim JJ. Exciplex-forming co-host for organic light-emitting diodes with ultimate efficiency. *Adv Funct Mater*. 2013;23(39):4914–49120.
47. Giebink NC, D'Andrade BW, Weaver MS, Brown JJ, Forrest SR. Direct evidence for degradation of polaron excited states in organic light emitting diodes. *J Appl Phys*. 2009;105(12):124514.
48. Lee JH, Chen CH, Lee PH, et al. Blue organic light-emitting diodes: current status, challenges, and future outlook. *J Mater Chem C*. 2019;7(20):5874–58788.
49. Kuma H, Hosokawa C. Blue fluorescent OLED materials and their application for high-performance devices. *Sci Technol Adv Mater*. 2014;15(3):034201.
50. Cok RS, Meitl M, Rotzoll R, et al. Inorganic light-emitting diode displays using micro-transfer printing. *J Soc Info Disp*. 2017;25(10):589–609.
51. Bibl A, Higginson JA, Law HF, Hu HH, inventors; LuxVue Technology Corp, assignee. Method of forming a micro light emitting diode array. United States patent US 8,426,227. April 23, 2013.
52. Wu MH, Fang YH, Chao CH, inventors; Industrial Technology Research Institute, PlayNitride Inc, assignee. Electric-programmable magnetic module and picking-up and placement process for electronic devices. United States patent US 9,607,907. March 28, 2017.
53. Ding K, Avrutin V, Izyumskaya N, Özgür Ü, Morkoç H. Micro-LEDs, a manufacturability perspective. *Appl Sci*. 2019;9(6):1206.
54. Delaporte P, Alloncle AP. Laser-induced forward transfer: a high resolution additive manufacturing technology. *Opt Laser Technol*. 2016;78:33–41.
55. Sasaki K, Schuele PJ, Ulmer K, Lee JJ, inventors; eLux Inc, assignee. System and method for the fluidic assembly of emissive displays. United States patent US 10,418,527. September 17, 2019.
56. Day J, Li J, Lie DY, Bradford C, Lin JY, Jiang HX. III-Nitride full-scale high-resolution microdisplays. *Appl Phys Lett*. 2011;99(3):031116.
57. Liang KL, Kuo WH, Shen HT, Yu PW, Fang YH, Lin CC. Advances in color-converted micro-LED arrays. *Jpn J Appl Phys*. 2020;60:SA0802.
58. Zhang L, Ou F, Chong WC, Chen Y, Li Q. Wafer-scale monolithic hybrid integration of Si-based IC and III-V epi-layers—a mass manufacturable approach for active matrix



- micro-LED micro-displays. *J Soc Inf Display*. 2018;26(3):137–145.
59. Nishimura J, Hara K, Daitoh T, et al. 3-1: Invited Paper: Super Bright 8K LCD with 10,000 nit realized by excellent light-resistance characteristics of IGZO TFT backplane. *SID Symp Dig Tech Pap*. 2020;51(1):1–4.
60. Lee JH, Zhu X, Lin YH, et al. High ambient-contrast-ratio display using tandem reflective liquid crystal display and organic light-emitting device. *Opt Express*. 2005;13(23):9431–9438.
61. Dobrowolski JA, Sullivan BT, Bajcar RC. Optical interference, contrast-enhanced electroluminescent device. *Appl Optics*. 1992;31(28):5988–5996.
62. Cok RS, inventor; Eastman Kodak Co, assignee. OLED display with circular polarizer. United States patent US 7,259,505. August 21, 2007.
63. Chen H, Tan G, Wu ST. Ambient contrast ratio of LCDs and OLED displays. *Opt Express*. 2017;25(26):33643–33656.
64. Poitras D, Kuo CC, Py C. Design of high-contrast OLEDs with microcavity effect. *Opt Express*. 2008;16(11):8003–8015.
65. Singh R, Unni KN, Solanki A. Improving the contrast ratio of OLED displays: an analysis of various techniques. *Opt Mater*. 2012;34(4):716–723.
66. Chiu TL, Lee JH, Hsiao YP, et al. Absorptive and conductive cavity cathode with silver nanoparticles for low-reflection organic light-emitting devices. *J Phys D Appl Phys*. 2011;44(9):095102.
67. Lau KC, Xie WF, Sun HY, Lee CS, Lee ST. Contrast improvement of organic light-emitting devices with Sm:Ag cathode. *Appl Phys Lett*. 2006;88(8):083507.
68. Cho H, Yoo S. Polarizer-free, high-contrast inverted top-emitting organic light emitting diodes: effect of the electrode structure. *Opt Express*. 2012;20(2):1816–1824.
69. Tamaki M, Nakamitsu S, Ito H, et al. A 200-ppi full color active matrix micro-LED display with low-temperature-poly-silicon TFT backplane. *Proc Int Disp Workshops*. 2019;26:429–432.
70. Brightness of commercial TV. Available online: <https://www.rtings.com/>
71. Someya J, Sugiura H. Evaluation of liquid-crystal-display motion blur with moving-picture response time and human perception. *J Soc Info Display*. 2007;15(1):79–86.
72. Igarashi Y, Yamamoto T, Tanaka Y, et al. 43.3: Summary of moving picture response time (MPRT) and futures. *SID Symp Dig Tech Pap*. 2004;35(1):1262–1265.
73. Kurita T. 35.1: Moving picture quality improvement for hold-type AM-LCDs. *SID Symp Dig Tech Pap*. 2001;32(1):986–989.
74. Peng F, Chen H, Gou F, et al. Analytical equation for the motion picture response time of display devices. *J Appl Phys*. 2017;121(2):023108.
75. Chen H, Peng F, Gou F, Lee YH, Wand M, Wu ST. Nematic LCD with motion picture response time comparable to organic LEDs. *Optica*. 2016;3(9):1033–1034.
76. Peng F, Huang Y, Gou F, et al. High performance liquid crystals for vehicle displays. *Opt Mater Express*. 2016;6(3):717–726.
77. Gou F, Chen H, Li MC, Lee SL, Wu ST. Motion-blur-free LCD for high-resolution virtual reality displays. *J Soc Inf Display*. 2018;26(4):223–228.
78. Wu ST. Nematic liquid crystal modulator with response time less than 100  $\mu$ s at room temperature. *Appl Phys Lett*. 1990;57(10):986–988.
79. Hirakata JI, Shingai A, Tanaka Y, Ono K, Furuhashi T. 35.2: Super-TFT-LCD for moving picture images with the blink backlight system. *SID Symp Dig Tech Pap*. 2004;32(1):990–993.
80. Yamamoto T, Sasaki S, Igarashi Y, Tanaka Y. Guiding principles for high-quality moving picture in LCD TVs. *J Soc Inf Display*. 2006;14(10):933–940.
81. Li CH, Lu SH, Lin SY, Hsieh TY, Wang KS, Kuo WH. 51-4: Invited Paper: Ultra-fast moving-picture response-time LCD for virtual reality application. *SID Symp Dig Tech Pap*. 2018;49(1):678–680.
82. Matsushima T, Kimura S, Komura S. Fast response in-plane switching liquid crystal display mode optimized for high-resolution virtual-reality head-mounted display. *J Soc Inf Display*. 2021;29(4):221–229.
83. Chen D, Liu B, Wang K, et al. 52-4: Late-News-Paper: Development of 240Hz refresh rate ADS mode gaming product. *SID Symp Dig Tech Pap*. 2020;51(1):773–776.
84. Lin CL, Chen FH, Wang MX, Lai PC, Tseng CH. Gate driver based on a-Si:H thin-film transistors with two-step-bootstrapping structure for high-resolution and high-frame-rate displays. *IEEE Trans Electron Devices*. 2017;64(8):3494–3497.
85. Wu YE, Lee MH, Lin YC, Kuo C, Lin YH, Huang WM. 41-1: Invited Paper: Active matrix mini-LED backlights for 1000PPI VR LCD. *SID Symp Dig Tech Pap*. 2019;50(1):562–565.
86. Murawski C, Leo K, Gather MC. Efficiency roll-off in organic light-emitting diodes. *Adv Mater*. 2013;25(47):6801–6827.
87. Virey EH, Baron N, Bouhamri Z. 11-3: Overlooked challenges for microLED displays. *SID Symp Dig Tech Pap*. 2019;50(1):129–132.
88. Templier F, Bernard J. 18-3: A new approach for fabricating high-performance microLED displays. *SID Symp Dig Tech Pap*. 2019;50(1):240–243.
89. Mun B-J, Lee G-D. The optical technology to improve the gamma-curve in liquid crystal display modes. *Mol Cryst Liq Cryst*. 2014;595(1):92–97.
90. Kim HJ, Lim YJ, Murali G, et al. Reduction of gamma distortion in oblique viewing directions in polymer-stabilized vertical alignment liquid crystal mode. *Curr Opt Photonics*. 2017;1(2):157–162.
91. Mori H. Novel optical compensators of negative birefringence for wide-viewing-angle twisted-nematic liquid-crystal displays. *Jpn J Appl Phys*. 1997;36(3R):1068–1072.
92. Kim K-H, Song J-G, Park S-B, Lyu J-J, Souk J-H, Lee K-H. PVA technology for high performance LCD monitors. *J Inf Display*. 2000;1(1):3–8.
93. Takeda A, Kataoka S, Sasaki T, et al. 41.1: A super-high image quality multi-domain vertical alignment LCD by new rubbing-less technology. *SID Symp Dig Tech Pap*. 1998;29(1):1077–1080.
94. Kim SS. 66.1: Invited Paper: The world's largest (82-in.) TFT-LCD. *SID Symp Dig Tech Pap*. 2005;36(1):1842–1847.
95. Tien K-C, Wu Y-C, Liao C-H, et al. 28.1: Premium picture quality by super-multi-domain polymer sustained alignment

- LCD technology. *SID Symp Dig Tech Pap.* 2012;43(1):371–374.
96. Hong Q, Wu TX, Zhu X, Lu R, Wu ST. Extraordinarily high-contrast and wide-view liquid-crystal displays. *Appl Phys Lett.* 2005;86(12):121107.
  97. Lu R, Hong Q, Wu ST, Peng KH, Hsieh HS. Quantitative comparison of color performances between IPS and MVA LCDs. *J Disp Technol.* 2006;2(4):319–326.
  98. Hofmann S, Thomschke M, Freitag P, Furno M, Lüssem B, Leo K. Top-emitting organic light-emitting diodes: influence of cavity design. *Appl Phys Lett.* 2010;97(25):278.
  99. Dong C, Fu X, Cao L, et al. Multi-mode organic light-emitting diode to suppress the viewing angle dependence. *ACS Appl Mater Interfaces.* 2020;12(28):31667–31676.
  100. Kim E, Chung J, Lee J, Cho H, Cho NS, Yoo S. A systematic approach to reducing angular color shift in cavity-based organic light-emitting diodes. *Org Electron.* 2017;48:348–356.
  101. Schwab T, Schubert S, Hofmann S, et al. Highly efficient color stable inverted white top-emitting OLEDs with ultrathin wetting layer top electrodes. *Adv Opt Mater.* 2013;1(10):707–713.
  102. Tan G, Lee JH, Lin SC, Zhu R, Choi SH, Wu ST. Analysis and optimization on the angular color shift of RGB OLED displays. *Opt Express.* 2017;25(26):33629–33642.
  103. Kim JB, Lee JH, Moon CK, Kim KH, Kim JJ. Highly enhanced light extraction from organic light emitting diodes with little image blurring and good color stability. *Org Electron.* 2015;17:115–120.
  104. Kim J, Qu Y, Coburn C, Forrest SR. Efficient outcoupling of organic light-emitting devices using a light-scattering dielectric layer. *ACS Photonics.* 2018;5(8):3315–3321.
  105. Xu K, Lu C, Huang Y, Hu J, Wang X. Enhanced outcoupling efficiency and removal of the microcavity effect in top-emitting OLED by using a simple vapor treated corrugated film. *RSC Adv.* 2017;7(86):54876–54880.
  106. Gou F, Hsiang EL, Tan G, et al. Angular color shift of micro-LED displays. *Opt Express.* 2019;27(12):A746–57.
  107. Choi HW, Jeon CW, Dawson MD, Edwards PR, Martin RW, Tripathy S. Mechanism of enhanced light output efficiency in InGaN-based microlight emitting diodes. *J Appl Phys.* 2003;93(10):5978–5982.
  108. Wang XH, Fu WY, Lai PT, Choi HW. Evaluation of InGaN/GaN light-emitting diodes of circular geometry. *Opt Express.* 2009;17(25):22311–22319.
  109. Yang SM, Wang PH, Chao CH, et al. Angular color variation in micron-scale light-emitting diode arrays. *Opt Express.* 2019;27(16):A1308–23.
  110. Biwa G, Doi M, Yasuda A, Kadota H. 11-1: Invited Paper: Technologies for the crystal LED display system. *SID Symp Dig Tech Pap.* 2019;50(1):121–124.
  111. Henry W, Percival C. 55-2: Invited Paper: ILED displays: next generation display technology. *SID Symp Dig Tech Pap.* 2016;47(1):747–750.
  112. Luo Z, Chen Y, Wu ST. Wide color gamut LCD with a quantum dot backlight. *Opt Express.* 2013;21(22):26269–26284.
  113. Donofrio RL. The Helmholtz-Kohlrausch effect. *J Soc Inf Display.* 2011;19(10):658–664.
  114. Available from <https://multimedia.3m.com/mws/media/12646000/3ms-display-quality-score-presentation-pdf.pdf>
  115. Zhu R, Luo Z, Chen H, Dong Y, Wu ST. Realizing Rec. 2020 color gamut with quantum dot displays. *Opt Express.* 2015;23(18):23680–23693.
  116. Jang E, Jun S, Jang H, Lim J, Kim B, Kim Y. White-light-emitting diodes with quantum dot color converters for display backlights. *Adv Mater.* 2010;22(28):3076–3080.
  117. Hosoumi S, Yamaguchi T, Inoue H, Nomura S, Yamaoka R, Sasaki T. Seo S. 3-4: Ultra-wide color gamut OLED display using a deep-red phosphorescent device with high efficiency, long life, thermal stability, and absolute BT.2020 red chromaticity. *SID Symp Dig Tech Pap.* 2017;48(1):13–16.
  118. Takita Y, Takeda K, Hashimoto N, et al. Highly efficient deep-blue fluorescent dopant for achieving low-power OLED display satisfying BT.2020 chromaticity. *J Soc Inf Display.* 2018;26(2):55–63.
  119. Bulashevich KA, Kulik AV, Karpov SY. Optimal ways of colour mixing for high-quality white-light LED sources. *Phys Status Solidi (a).* 2015;212(5):914–919.
  120. Guo W, Chen N, Lu H, et al. The impact of luminous properties of red, green, and blue mini-LEDs on the color gamut. *IEEE Trans Electr Dev.* 2019;66(5):2263–2268.
  121. Chu CH, Wu F, Sun S. 31.2: High PPI micro-LED display based on PWM technology. *SID Symp Dig Tech Pap.* 2018;49(S1):337–338.
  122. Tamaki M, Suzuki T, Aoki K, et al. Matsuda S. 9-5: Late-News Paper: A 3.9-inch LTPS TFT full color microLED display with novel driving and reflector cavity process. *SID Symp Dig Tech Pap.* 2020;51(1):111–114.
  123. Oh JH, Lee KH, Yoon HC, Yang H, Do YR. Color-by-blue display using blue quantum dot light-emitting diodes and green/red color converting phosphors. *Opt Express.* 2014;22(102):A511–20.
  124. Han HV, Lin HY, Lin CC, et al. Resonant-enhanced full-color emission of quantum-dot-based micro LED display technology. *Opt Express.* 2015;23(25):32504–32515.
  125. Yin Y, Hu Z, Ali MU, et al. Full-color micro-LED display with CsPbBr<sub>3</sub> perovskite and CdSe quantum dots as color conversion layers. *Adv Mater Technol.* 2020;5(8):2000251.
  126. Hu Z, Yin Y, Ali MU, et al. Inkjet printed uniform quantum dots as color conversion layers for full-color OLED displays. *Nanoscale.* 2020;12(3):2103–2110.
  127. Chen GS, Wei BY, Lee CT, Lee HY. Monolithic red/green/blue micro-LEDs with HBR and DBR structures. *IEEE Photon Technol Lett.* 2017;30(3):262–265.
  128. Hsiang EL, Li Y, He Z, et al. Enhancing the efficiency of color conversion micro-LED display with a patterned cholesteric liquid crystal polymer film. *Nanomaterials.* 2020;10(12):2430.
  129. Chu SY, Wang HY, Lee CT, et al. Improved color purity of monolithic full color micro-LEDs using distributed Bragg reflector and blue light absorption material. *Coatings.* 2020;10(5):436.
  130. He J, Chen H, Chen H, Wang Y, Wu ST, Dong Y. Hybrid downconverters with green perovskite-polymer composite films for wide color gamut displays. *Opt Express.* 2017;25(11):12915–12925.
  131. Liu YT, Liao KY, Lin CL, Li YL. 66-2: Invited Paper: PixeLED display for transparent applications. *SID Symp Dig Tech Pap.* 2018;49(1):874–875.

132. Ko YH, Prabhakaran P, Choi S, Kim GJ, Lee C, Lee KS. Environmentally friendly quantum-dot color filters for ultra-high-definition liquid crystal displays. *Sci Rep.* 2020;10:15817. <https://doi.org/10.1038/s41598-020-72468-8>
133. Koch KW, Hathaway B, Kosik Williams C, et al. Anti-reflection displays with ambient contrast enhancement for extended device battery lifetime and reduced energy consumption. *J Soc Inf Display.* 2020;28(10):801–807.
134. Hsiang EL, He Z, Huang Y, Gou F, Lan YF, Wu ST. Improving the power efficiency of micro-LED displays with optimized LED chip sizes. *Crystals.* 2020;10(6):494.
135. Smith JM, Ley R, Wong MS, et al. Comparison of size-dependent characteristics of blue and green InGaN micro-LEDs down to 1  $\mu\text{m}$  in diameter. *Appl Phys Lett.* 2020;116(7):071102.
136. Olivier F, Tirano S, Dupré L, Aventurier B, Largeron C, Templier F. Influence of size-reduction on the performances of GaN-based micro-LEDs for display application. *JOL.* 2017; 191:112–116.
137. Konoplev SS, Bulashevich KA, Karpov SY. From large-size to micro-LEDs: scaling trends revealed by modeling. *Phys Status Solidi a.* 2018;215(10):1700508.
138. Oh JT, Lee SY, Moon YT, et al. Light output performance of red AlGaInP-based light emitting diodes with different chip geometries and structures. *Opt Express.* 2018;26(9): 11194–11200.
139. Ahmed K. 11-2: Micro LEDs efficiency targets for displays. *SID Symp Dig Tech Pap.* 2019;50(1):125–128.
140. Jung T, Choi JH, Jang SH, Han SJ. 32-1: Invited Paper: Review of micro-light-emitting-diode technology for micro-display applications. *SID Symp Dig Tech Pap.* 2019;50(1): 442–446.
141. Möller S, Forrest SR. Improved light out-coupling in organic light emitting diodes employing ordered microlens arrays. *J Appl Phys.* 2002;91(5):3324–3327.
142. Madigan CF, Lu MH, Sturm JC. Improvement of output coupling efficiency of organic light-emitting diodes by backside substrate modification. *Appl Phys Lett.* 2000;76(13): 1650–1652.
143. Yang CJ, Liu SH, Hsieh HH, Liu CC, Cho TY, Wu CC. Microcavity top-emitting organic light-emitting devices integrated with microlens arrays: simultaneous enhancement of quantum efficiency, cd/A efficiency, color performances, and image resolution. *Appl Phys Lett.* 2007;91(25):253508.
144. Jeon S, Jeong JH, Song YS, Jeong WI, Kim JJ, Youn JR. Vacuum nano-hole array embedded organic light emitting diodes. *Nanoscale.* 2014;6(5):2642–2648.
145. Ou QD, Zhou L, Li YQ, et al. Extremely efficient white organic light-emitting diodes for general lighting. *Adv Funct Mater.* 2014;24(46):7249–7256.
146. Lin HY, Ho YH, Lee JH, et al. Patterned microlens array for efficiency improvement of small-pixelated organic light-emitting devices. *Opt Express.* 2008;16(15):11044–11051.
147. Do YR, Kim YC, Song YW, et al. Enhanced light extraction from organic light-emitting diodes with 2D  $\text{SiO}_2/\text{SiN}_x$  photonic crystals. *Adv Mater.* 2003;15(14):1214–1218.
148. Chen YJ, Lee WK, Chen YT, et al. A vision toward ultimate optical out-coupling for organic light-emitting diode displays: 3D pixel configuration. *Adv Sci.* 2018;5(10):1800467.
149. Jonza JM, Weber MF, Ouderkirk AJ, Stover CA, inventors; 3M Innovative Properties Co, assignee. Polarizing beam-splitting optical component. United States patent US 5,962,114. October 5, 1999.
150. Hulze HG, de Greef P. 51.3: Driving an adaptive local dimming backlight for LCD-TV systems. *SID Symp Dig Tech Pap.* 2008;39(1):772–775.
151. Bulashevich KA, Konoplev SS, Karpov SY. Effect of die shape and size on performance of III-nitride micro-LEDs: a modeling study. *Photonics.* 2018;5(4):41.
152. Chen Z, Yan S, Danesh C. MicroLED technologies and applications: characteristics, fabrication, progress, and challenges. *J Phys D Appl Phys.* 2021;54:123001.
153. Lee HS, Jang S, Noh J, et al. 28-4L: Late-News Paper: An ultra high density 1.96" UHD 2250ppi display. *SID Symp Dig Tech Pap.* 2017;48(1):403–405.
154. Castles F, Morris SM, Gardiner DJ, Malik QM, Coles HJ. Ultra-fast-switching flexoelectric liquid-crystal display with high contrast. *J Soc Inf Display.* 2010;18(2):128–133.
155. Chen CH, Lin FC, Hsu YT, Huang YP, Shieh HP. A field sequential color LCD based on color fields arrangement for color breakup and flicker reduction. *J Display Technol.* 2009; 5(1):34–39.
156. Lin FC, Huang YP, Wei CM, Shieh HP. Color-breakup suppression and low-power consumption by using the Stencil-FSC method in field-sequential LCDs. *J Soc Inf Display.* 2009; 17(3):221–228.
157. Lu P, Huang G, Yang S, et al. 52-4: Highest PPI micro-OLED display sustain for near-eye application. *SID Symp Dig Tech Pap.* 2019;50(1):725–726.
158. Ghosh A, Donoghue EP, Khayrullin I, et al. 62-1: Invited Paper: Directly patterned 2645 PPI full color OLED micro-display for head mounted wearables. *SID Symp Dig Tech Pap.* 2016;47(1):837–840.
159. Joo WJ, Kyoung J, Esfandyarpour M, et al. Metasurface-driven OLED displays beyond 10,000 pixels per inch. *Science.* 2020; 370(6515):459–463.
160. Zhang L, Ou F, Chong WC, Chen Y, Zhu Y, Li Q. 31.1: Invited Paper: Monochromatic active matrix micro-LED micro-displays with >5,000 dpi pixel density fabricated using monolithic hybrid integration process. *SID Symp Dig Tech Pap.* 2018;49(S1):333–336.
161. Kawanishi H, Onuma H, Maegawa M, et al. High-resolution and high-brightness full-colour "Silicon Display" for augmented and mixed reality. *J Soc Inf Display.* 2021;29(1):57–67.
162. Templier F. GaN-based emissive microdisplays: a very promising technology for compact, ultra-high brightness display systems. *J Soc Inf Display.* 2016;24(11):669–675.
163. Mini-LED LCD cost forecast. Available online: <https://omdia.tech.informa.com/OM006957/Display-Dynamics-TCL-has-a-new-low-cost-mini-LED-backlight-LCD-TV-with-FALD-technology>
164. Lewis JS, Weaver MS. Thin-film permeation-barrier technology for flexible organic light-emitting devices. *IEEE J Sel Top Quantum Electron.* 2004;10(1):45–57.
165. Kondakov DY, Sandifer JR, Tang CW, Young RH. Non-radiative recombination centers and electrical aging of organic light-emitting diodes: direct connection between

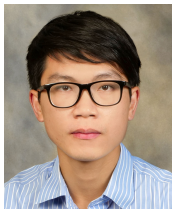


- accumulation of trapped charge and luminance loss. *J Appl Phys.* 2003;93(2):1108–1119.
166. Scholz S, Kondakov D, Lussem B, Leo K. Degradation mechanisms and reactions in organic light-emitting devices. *Chem Rev.* 2015;115(16):8449–8503.
  167. Zhang Y, Lee J, Forrest SR. Tenfold increase in the lifetime of blue phosphorescent organic light-emitting diodes. *Nat Commun.* 2014;5:5008.
  168. Lee J, Jeong C, Batagoda T, Coburn C, Thompson ME, Forrest SR. Hot excited state management for long-lived blue phosphorescent organic light-emitting diodes. *Nat Commun.* 2017;8:15566.
  169. Lin BY, Lee MZ, Tseng PC, et al. P-174: 16.1-times elongation of operation lifetime in a blue TTA-OLED by using new ETL and EML materials. *SID Symp Dig Tech Pap.* 2017;48(1):1928–1931.
  170. Lin BY, Easley CJ, Chen CH, et al. Exciplex-sensitized triplet-triplet annihilation in heterojunction organic thin-film. *ACS Appl Mater Interfaces.* 2017;9(12):10963–10970.
  171. Goto S, Miyatake M, Saiki Y. 40-1: Distinguished Paper: A novel ultra-thin polarizer to achieve thinner and moreflexible displays. *SID Symp Dig Tech Pap.* 2016;47(1):510–513.
  172. Liang J, Li L, Niu X, Yu Z, Pei Q. Elastomeric polymer light-emitting devices and displays. *Nat Photonics.* 2013;7(10):817–824.
  173. Harding MJ, Horne IP, Yaglioglu B. 53-2: Invited Paper: Flexible LCDs enabled by OTFT. *SID Symp Dig Tech Pap.* 2017;48(1):793–876.
  174. Sher CW, Chen KJ, Lin CC, et al. Large-area, uniform white light LED source on a flexible substrate. *Opt Express.* 2015;23(19):A1167–78.

## AUTHOR BIOGRAPHIES



**En-Lin Hsiang** received his BS and MS degrees from National Chiao Tung University, Hsinchu, Taiwan, in 2014 and 2016, respectively. Currently, he is working toward the PhD degree at College of Optics and Photonics, University of Central Florida, USA. His current research focuses on micro-LED and mini-LED displays.



**Zhiyong Yang** received his BS degree in Optoelectronic Engineering from Chongqing University in 2017 and is currently working toward a PhD degree from the College of Optics and Photonics, University of Central Florida. His current research interests include liquid crystal-based sensors, mini-LED backlight, OLED display, and micro-LED display.



**Qian Yang** received his BS degree in Physics from Nanjing University in 2017 and MS degree in Physics from University of Rochester in 2019. He is currently working toward a PhD degree from the College of Optics and Photonics, University of Central Florida. His current research interests include liquid crystal spatial light modulators for LiDAR applications, planar optics for AR/VR displays, and mini-LED and micro-LED displays.



**Yi-Fen Lan** received his PhD degree from National Taiwan University in 2010. Currently, he is a principal engineer at AU Optronics Corporation. His research interests include high-dynamic-range LCDs and micro-LED displays. Dr. Yi-Fen Lan is principal engineer at AU Optronics. He received his PhD on Polymer Science from National Taiwan University (2010). He was a visiting scholar at Prof. Shin-Tson Wu's Lab (University of Central Florida, USA) in 2013 and visiting scientist at Prof. Daping Chu's Lab (University of Cambridge, UK) in 2014. His research interests include polymer-stabilized blue phase liquid crystal display and micro-LED display. Presently, he focuses on mass transfer and mass repair of micro-LED manufacturing.



**Shin-Tson Wu** is Pegasus Professor at the College of Optics and Photonics, University of Central Florida. He is among the first six inductees of the Florida Inventors Hall of Fame (2014) and a Charter Fellow of the National Academy of Inventors (2012). He is a Fellow of the IEEE, OSA, SID, and SPIE and an honorary Professor at Nanjing University (2013) and at National Chiao Tung University (2018). He is the recipient of 2014 OSA Esther Hoffman Beller Medal, 2011 SID Slottow-Owaki Prize, 2010 OSA Joseph Fraunhofer Award, 2008 SPIE G. G. Stokes Award, and 2008 SID Jan Rajchman Prize.

**How to cite this article:** Hsiang E-L, Yang Z, Yang Q, Lan Y-F, Wu S-T. Prospects and challenges of mini-LED, OLED, and micro-LED displays. *J Soc Inf Display.* 2021;29:446–465. <https://doi.org/10.1002/jsid.1058>